SEDIMENTOLOGY the journal of the International Association of Sedimentologists IAS

Sedimentology (2025) doi: 10.1111/sed.70076

Coastal engineering structures bifurcate intertidal eco-morphodynamic trajectories in a sediment-starved delta

JIE WANG*,†, ZHIJUN DAI*, XUEFEI MEI*, HUAN-FENG DUAN†, JINPING CHENG‡, JAAP H. NIENHUIS§, XIXING LIANG*, JIEJUN LUO* and SERGIO FAGHERAZZI¶

**State Key Laboratory of Estuarine and Coastal Research, East China Normal University, Shanghai, China (E-mail: zjdai@sklec.ecnu.edu.cn)*

†State Key Laboratory of Climate Resilience for Coastal Cities, Department of Civil and Environmental Engineering, The Hong Kong Polytechnic University, Hong Kong, China

‡Department of Science and Environmental Studies, The Education University of Hong Kong, Hong Kong, China

§Department of Physical Geography, Faculty of Geosciences, Utrecht University, Utrecht, the Netherlands

¶Department of Earth and Environment, Boston University, Boston, MA, USA

Associate Editor – Massimiliano Ghinassi

ABSTRACT

Damming has reduced sediment supply to most river deltas, impairing the land-building capacity and ecological services of tidal wetlands. How localised engineering structures, coupled with sediment starvation, drive shifts in intertidal ecology and morphodynamics within a deltaic system remains a critical knowledge gap. Here, high-resolution Unmanned Aerial Vehicle imagery and Terrestrial Laser Scanner topographic data are integrated to quantify the dynamics of the Nanhui wetlands, the largest marginal wetland in the Yangtze Delta, where riverine sediment input has decreased by more than 70% in the last decades. Results show that the total salt marsh area expanded from 21.80 ha in 2019 to 46.37 ha in 2022, with the area of native and invasive marsh species increasing by 58.5% and 221.1%, respectively. The salt marsh in the East Nanhui wetland rapidly increased, growing 7.2-fold to reach 31.25 ha, whereas the salt marsh extent in the South Nanhui wetland declined by 16%, shrinking to 15.12 ha. Groins promoting siltation in the East Nanhui wetland weakened the wave and tidal forcing. This facilitated the accumulation of sediment from coarser-grained sources, as well as the encroachment of native *Scirpus mariqueter*. On the contrary, following the reclamation of the upper intertidal and supratidal zones, the South Nanhui wetland suffered severe retreat and sustained coarsening of bed sediment, due to enhanced alongshore currents and waves. Sediment remobilised by erosion deposited in the high marsh, favouring the invasion of *Spartina alterniflora*. Hence, this study clarifies that anthropogenic effects coupled with changes in hydrodynamic regimes can bifurcate the intertidal eco-morphodynamics into two distinct states: prograding versus eroding. Reduced sediment availability is likely to increase erosion of native salt marshes, thereby favouring the encroachment of invasive high marsh vegetation. Our findings highlight the value of high-resolution measurements in revealing different trajectories of nature-based solutions for coastal protection in mega-deltas.

Keywords Engineering structure, intertidal eco-morphodynamics, salt marsh, sediment starvation, UAV-TLS integration, Yangtze (Changjiang) Delta.

INTRODUCTION

Deltaic wetlands develop at the land-ocean interface, providing critical ecological services and resistance to coastal storms (Michener *et al.*, 1997; Möller *et al.*, 2014; Temmerman *et al.*, 2023). The eco-morphodynamics of intertidal salt marshes and bare flats are regulated by multiple factors, including fluvial sediment inputs, local hydrodynamic conditions and human activities (Friedrichs & Perry, 2001; Coco *et al.*, 2013; Kirwan & Megonigal, 2013; Bádenas *et al.*, 2018). However, declining upstream sediment supply, sea-level rise (SLR) and local coastal engineering structures (e.g. seawalls, groins, revetments and breakwaters) can jeopardise the morphodynamic stability and ecological resilience of tidal wetlands in many mega-deltas worldwide (Gedan *et al.*, 2009; FitzGerald & Hughes, 2019; Nienhuis *et al.*, 2020). Therefore, assessing eco-morphodynamic variations in vulnerable salt marshes and bare flats under multiple natural and anthropogenic pressures is a key priority for coastal communities.

External physical and biological disturbances tend to exacerbate the divergent trajectories of change of a deltaic system, which could induce ecosystem instability due to eco-morphodynamic feedbacks (Allen, 2000; D'Alpaos, 2011; Ghinassi *et al.*, 2018; Schuerch *et al.*, 2019). For example, vegetation zonation of intertidal salt marshes is a primary signature of eco-morphodynamic feedbacks (Silvestri *et al.*, 2005; Fagherazzi *et al.*, 2012; Chirol *et al.*, 2021; Finotello *et al.*, 2023). Physicochemical gradients, such as spatial variations in wave power, tidal forcing, suspended sediment concentration (SSC), salinity and nutrient availability, may trigger growth, mortality and fragmentation of salt marshes, which in turn affects intertidal erosion, deposition and hydrodynamics (Phillips, 2018; van Regteren *et al.*, 2020; Wei *et al.*, 2022, 2024). In recent decades, fluvial sediment supply to major river deltas has decreased by approximately 50%, leading to significant erosion and the retreat of deltaic tidal wetlands (Murray *et al.*, 2019; Syvitski *et al.*, 2022; Li *et al.*, 2024; Wang *et al.*, 2025a). Meanwhile, rapid SLR is projected to cause a 78% loss of coastal wetlands by 2100, with stronger coastal storms possibly exacerbating the long-term degradation of the salt marsh ecosystems (Kirwan & Mudd, 2012; Spencer *et al.*, 2016; Törnqvist *et al.*, 2021; Shi *et al.*, 2025). Moreover, invasive marsh species can outcompete native vegetation, significantly disrupting the ecological structure and functions of deltaic wetlands (Jiang *et al.*, 2009; Phillips, 2018; Fagherazzi *et al.*, 2020; Day *et al.*, 2024).

The effects of high-intensity human activities on the eco-morphodynamic trajectories of deltaic tidal wetlands remain poorly understood, particularly regarding the facilitation of invasive salt marsh species with greater interspecific competitiveness than native marsh vegetation. Thus, there is an urgent need to conduct comprehensive field observations by utilising advanced techniques. These observations are important for salt marshes and bare flats in low-lying, sediment-starved deltas that are characterised by extensive engineering structures (Conery *et al.*, 2020; Granse *et al.*, 2021; Agrillo *et al.*, 2023; Ensign *et al.*, 2023). In particular, spatial differences in geomorphology and salt marsh vegetation across intertidal areas within a deltaic system have not been well quantified, largely owing to the lack of high-precision field monitoring data.

Nowadays, both Unmanned Aerial Vehicles (UAVs) and Terrestrial Laser Scanners (TLSs) are increasingly being employed to detect changes in forest ecosystems, land use types and topographic features (Mancini *et al.*, 2013; Tong *et al.*, 2015; Calders *et al.*, 2020). Compared to satellite remote sensing (such as Landsat, Sentinel, etc.), UAVs can cost-effectively acquire centimetre-resolution orthophotos with fewer weather-related limitations (Pinton *et al.*, 2021; Agrillo *et al.*, 2023). TLSs, by contrast, can detect the spatial distances to target points by actively emitting laser beams and generating high-density, geo-referenced 3D point clouds over a range of several kilometres (Fabbri *et al.*, 2017; Conery *et al.*, 2020; Wang *et al.*, 2022a). Therefore, UAVs and TLSs allow rapid acquisitions of large-scale vegetation distribution and

elevation data, especially in areas with low accessibility (Curcio *et al.*, 2023; van der Wal *et al.*, 2023). Few studies have integrated UAV and TLS data to analyse the eco-morphodynamic changes of salt marshes and bare flats on an interannual scale, while also accounting for differences in these changes across distinct intertidal zones. This research gap is particularly crucial for rapidly evolving deltaic wetlands, as such findings are essential for assessing the effectiveness of nature-based coastal protection strategies and guiding tidal wetland restoration efforts.

The Yangtze (Changjiang) River is the largest river in Asia (Fig. 1A). Since the 1950s, the annual water discharge and suspended sediment load delivered to the delta have averaged 8.98×10^{11} m^3 and 3.51×10^8 t, respectively (CWRC, 2023). Approximately half of this fluvial sediment accumulates in the delta, forming large-scale tidal flats, shoals and a subaqueous delta, while the delta itself develops a network of bifurcated channels (Fig. 1B; Chen *et al.*, 1988; Hori *et al.*, 2001). More than one-third of the upstream sediment supply is transported through the South Passage to subaqueous and offshore areas, where mouth bars form under saltwater-freshwater mixing (Yun, 2004). In recent years, reduced sediment input from the Yangtze River following upstream dam construction has triggered severe erosion of tidal flats, deep channels and the delta front, particularly during high-runoff periods in the flood season (Dai *et al.*, 2014, 2018a; Wang *et al.*, 2022b). Erosion has become the greatest threat to the sustainability of tidal wetlands in the mega-Yangtze Delta (Dai *et al.*, 2018a, 2018b; Lou *et al.*, 2025). In addition, land reclamation and dredging of navigation channels have further disrupted the hydrodynamic regimes and sediment budgets within the delta system, which is highly likely to induce intertidal eco-morphodynamic feedbacks distinct from those in natural states (Luan *et al.*, 2017; Guo *et al.*, 2021; van Maren *et al.*, 2025).

The Nanhui Wetland is the largest marginal wetland in the Yangtze Delta, and provides a significant ecological buffer against storms (Fig. 1B). Large-scale reclamation projects covering 150 km^2 replaced extensive tidal flats between 1994 and 2008, and siltation-promoting engineering structures have been constructed in the northern part since 2014 (Yun, 2004; Li *et al.*, 2010; Wang *et al.*, 2024). Thus, this area was selected here to investigate intertidal eco-morphodynamic changes under reduced upstream sediment inputs and intense anthropogenic disturbances (Fig. 1C). Our primary objectives are as follows: (1) to clarify the differences in sedimentary shifts and erosion-accretion geomorphic patterns across different parts of the Nanhui Wetland based on TLS-acquired topographic data; (2) to quantify the annual spatio-temporal dynamics of the distribution and extent of native and invasive salt marsh species using UAV orthoimages; (3) to propose conceptual models of intertidal eco-morphodynamics driven by engineering structures in the sediment-starved Nanhui wetland. The results and findings presented herein may offer valuable support for a better understanding of intertidal eco-morphodynamic feedbacks and ecological restorations in deltas under reduced fluvial sediment supply and strong anthropogenic stress.

STUDY AREA

Abundant riverine sediment supply has driven the accretion and progradation of the Yangtze Delta over the last two millennia (Hori *et al.*, 2001; Fan *et al.*, 2017; Dai *et al.*, 2018a). The Nanhui Wetland is located in the southern Yangtze Delta, bordering the Yangtze South Passage and Hangzhou Bay, with isobaths extending in a smooth arc towards the submerged delta (Fig. 1B). The Nanhui Wetland's shoreline is characterised by a distinct seaward protrusion, with two dominant orientations: north–south (N–S) and northeast–southwest (NE–SW) (Fig. 1C). Notably, the width of its tidal flats gradually narrows from north to south. The tide is semi-diurnal, with a mean tidal range of 3.26 m and a maximum tidal range of 5.92 m at Luchaogang (Fig. 1B; Yun, 2004). Flooding tidal currents propagate shoreward and split into two major sub-currents outside of the Nanhui protrusion: one flows towards the upstream distributary of the Yangtze Delta (along the northern margin of the Nanhui Wetland), while the other extends towards Hangzhou Bay (along the southern margin of the Nanhui Wetland). In contrast, ebbing tidal currents converge at the Nanhui shoreline protrusion (Chen *et al.*, 1999). Therefore, based on its hydro-topographic characteristics, the Nanhui wetland is typically divided into eastern and southern parts, that is the East Nanhui wetland and South Nanhui wetland (Fig. 1C). Waves in the study area are dominated

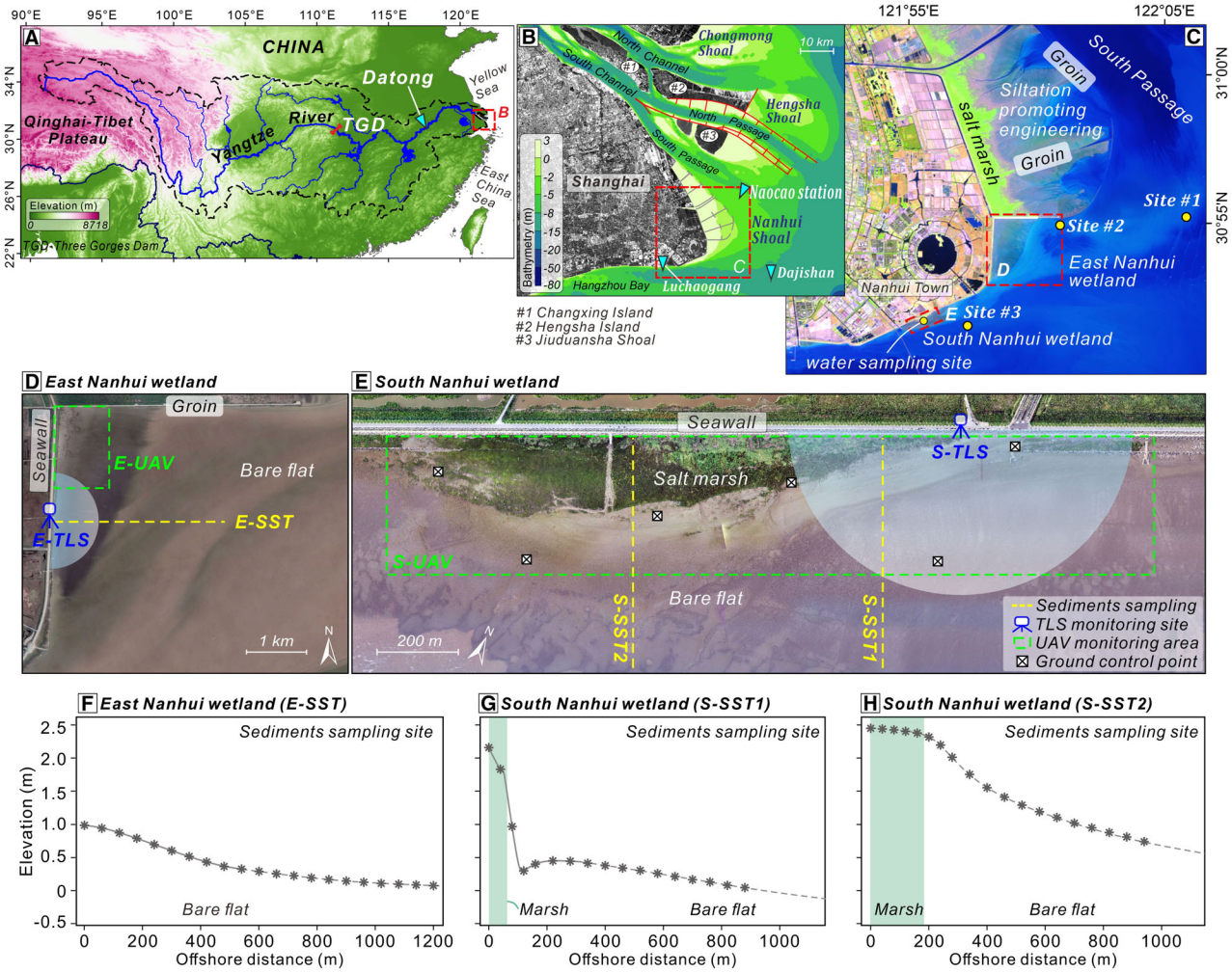

Fig. 1. Map of the study area. (A) Location of the Yangtze (Changjiang) River and distributaries in China, showing the Three Gorges Dam (TGD, the largest hydraulic project in the world) and Datong station (tidal limit). (B) Bathymetry of the Yangtze Delta, with the Nanhui wetlands situated in the southern portion of the delta, indicating three hydrological stations (Nancao, Luchaogang and Dajisha). (C) A remote sensing map of the East and South Nanhui wetlands shows that the northern groins were constructed in 2015 to promote coastal siltation. The locations of the intertidal water sampling and the three offshore hydrodynamic observation sites (#1 to #3) are shown. (D–E) Locations of the two UAV (Unmanned Aerial Vehicle) monitoring ranges, two TLS (Terrestrial Laser Scanner) observation sites, and three intertidal surficial sediment sampling transects established in the East Nanhui wetland and South Nanhui wetland. (F–H) Distribution of sediment sampling sites along the three transects in two wetlands.

by wind waves, which account for 80% of the total wave occurrences. Specifically, SE waves are dominant in summer, while NE-NNE waves prevail in winter, with a mean wave height of 0.8 m recorded at Dajishan station (Fig. 1B; Li, 1991; Chen *et al.*, 2001). Monsoons and storms trigger waves that tend to enhance the resuspension of intertidal bed sediments, producing erosion in the Nanhui Wetland (Dai *et al.*, 2008; Wang *et al.*, 2024). Historically, such land-sea hydrodynamic regimes have favoured landward sediment accretion, thereby promoting the rapid progradation of deltaic land (Hori *et al.*, 2001; Fan *et al.*, 2017; Dai *et al.*, 2018b).

Since the 1990s, rapid urbanisation in Shanghai has increased the demand for land. As a result, the supratidal and intertidal zones of the Nanhui wetland have been reclaimed, covering a total of 300 km^2 (Wei *et al.*, 2019; Zhang *et al.*,

Table 1. Data categories and their corresponding dates collected in the Nanhui wetlands, Yangtze Delta.

Area	East Nanhui wetland	South Nanhui wetland
UAV	July 22, 2019; July 30, 2022	July 24, 2018, July 18, 2019, July 18, 2022
TLS	April 20, 2018; December 15, 2021; December 15, 2022	January 23, 2019; January 4, 2021; December 15, 2021
Surficial sediment	April 20, 2018; November 10, 2018; October 17, 2019; December 15, 2021; July 30, 2022; December 15, 2022	S-SST1: February 5, 2018; January 23, 2019; January 12, 2020; January 8, 2022; December 15, 2022; S-SST2: September 28, 2019; January 23, 2020; January 8, 2022; August 18, 2022
Suspended sediment	\	July 18, 2019, to March 16, 2022
Field photographs	From 2017 to 2022	From 2017 to 2022

2020). Moreover, the invasive marsh species *Spartina alterniflora* was introduced in the Jiuduansha Wetlands in 1979 (Fig. 1B), adjacent to the Nanhui Wetland, aiming to increase local intertidal sedimentation rates and vegetation cover in the Yangtze Delta (He *et al.*, 2007; Huang & Zhang, 2007). Since then, *Spartina alterniflora* has expanded rapidly and gradually replaced native salt marsh species (i.e. *Scirpus mariqueter*) across many intertidal areas. Groins were constructed in 2014 in the northern part of the Nanhui Wetland to promote intertidal siltation, modifying local sedimentary and geomorphic processes and possibly promoting the encroachment of invasive marsh species (Fig. 1C; Wei *et al.*, 2020; Wang *et al.*, 2024).

DATA ACQUISITIONS AND METHODS

UAV-based salt marsh orthophotography

A UAV (*Phantom 4 RTK*, *DJI*) equipped with a single-lens visible-light sensor was used to acquire high-resolution (about 3 cm pixel^{-1}) image tiles of salt marshes and to analyse their dynamics. Two monitoring areas were established in the East Nanhui and South Nanhui wetlands (i.e. E-UAV and S-UAV) to encompass diverse salt marsh growth conditions (Fig. 1D and E). This UAV enhances positioning accuracy via connection to the CORS (Continuously Operating Reference Stations), enabling the acquisition of centimetre-accurate target image tiles. This system offers low cost and facilitates easy revisit (Pinton *et al.*, 2021; Curcio *et al.*, 2023). During each field survey, the flight height was set to 60 to 80 m to ensure higher spatial resolution, and the longitudinal and lateral overlap rates were fixed at 70% and 80%, respectively (Liang *et al.*, 2024).

Given that the planted invasive marsh vegetation in the East Nanhui wetland was confined to the interior of the breakwater and had almost occupied the entire enclosed area before 2019, its dynamics were rarely disrupted by changes in external driving forces. After 2019, sparse patches of native pioneer marsh vegetation began colonising the bare flats outside the breakwater. Thus, UAV data for the East Nanhui wetland were collected in July 2019 and July 2022 to document this vegetation encroachment (Table 1). For the South Nanhui wetland, the invasive marsh vegetation within the breakwater exhibited an accelerated seaward expansion trend starting in 2018, with its expansion reaching a peak in the summer of 2022. Subsequently, large-scale invasive salt marsh removal projects were implemented in the Yangtze Delta and the other coastal areas of China, aiming to restore the intertidal ecological functions dominated by native species. Hence, UAV data for the South Nanhui wetland were acquired in July 2018, July 2019 and August 2022, respectively (Table 1).

A total of six ground control points (GCPs) (Fig. 1E) were deployed in the southern study area, and RTK-measured elevations were used for orthorectification (Mancini *et al.*, 2013; Pinton *et al.*, 2021). Following image acquisition,

all UAV images were processed in Pix4Dmapper. Via the structure-from-motion (SfM) workflow, we generated digitally orthophotos of the salt marshes for the East and South Nanhui wetlands. Finally, a supervised classification approach was applied using QGIS to categorise the salt marsh vegetation into native and invasive species. The resulting classifications were rigorously validated by visual inspection and comparison with field-verified patches, which confirmed that the overall accuracy exceeded 90%. Based on these high-accuracy marsh classifications, the areas of each species were quantified, and their spatial changes were statistically analysed over different monitoring periods.

Surficial sediment collections and grain-size measurements

Intertidal surficial sediments were collected along one transect in the East Nanhui wetland and two transects in the South Nanhui wetland. The eastern transect (i.e. E-SST) extended gradually seaward from the breakwater to the bare flat, featured a gentle slope and lacked any salt marsh coverage (Fig. 1D). Sampling sites along this transect were spaced at 60 m intervals, with the maximum lateral length reaching 1200 m (Fig. 1F). Intertidal surficial sediments (collected from the top 0.5 cm layer) were sampled using hard-plastic corers and were subsequently placed into labelled, zip-sealed plastic bags. In total, six sets of sediment samples were collected along the E-SST transect, spanning from April 2018 to December 2022 (Table 1). Meanwhile, two sediment sampling transects were set in the South Nanhui wetland, designated as S-SST1 and S-SST2 (Fig. 1E). A narrow strip of invasive salt marsh vegetation was present on the seawall side of transect S-SST1, with a steep topographic slope at the marsh front that extended to the middle of the bare flats. In contrast, transect S-SST2 spanned a wider expanse of salt marsh, with gently sloping bare flats. Along these two transects, the sampling intervals for the five landward sites were 40 m, with 60 m intervals for the remaining seaward sites (Fig. 1G and H). Both transects had a maximum length exceeding 900 m and traversed the entire intertidal zone during the lowest tidal levels of spring tides. Surficial sediment samples were collected five times along S-SST1 and four times along S-SST2 between February 2018 and December 2022. Moreover, from July 2019 to March 2022, monthly suspended water samples were collected at the seaward-most site on the S-SST1 site during low tide, 18 samples in total (Fig. 1C).

All collected sediment samples were pre-treated for grain-size measurements. 5 ml of 10% H_2O_2 and 5 ml of 10% hydrochloric acid (HCl) were added to the sediment mixture to remove residual organic matter and calcium carbonate. More detailed sediment pre-treatment procedures were described in Wang *et al.* (2024). Lastly, we added 5 ml of 5% sodium hexametaphosphate to pre-treatment completed samples, and the mixture was then placed in an ultrasonic oscillator for 20 min to fully disperse sediment particles. The Dynamic Image Analysis of Camsizer XT (*Microtrac Retsch GmbH, Germany*) and the moment methods statistics (McManus, 1988) were used to calculate sediment average grain size, sorting coefficient and skewness. Additionally, the SSC was measured as the ratio of the dry weight of sediment to the total volume of sampled water.

Intertidal elevation and geomorphic change measured by TLS

Two TLS (*Riegl VZ-4000*, *Austria*) monitoring sites (i.e. the E-TLS and S-TLS) were set up on the seawalls to ensure an unobstructed view, facilitating the acquisition of high-density 3D point cloud data of intertidal surfaces (Fig. 1D and E). The TLS was configured with a pulse repetition rate of 150 kHz and a detection accuracy of about 15 mm (http://www.riegl.com). Its vertical and horizontal observation ranges were set to 60° and 360°, respectively, with corresponding vertical and horizontal resolutions of 0.004° and 0.03° (Wang *et al.*, 2022a). To minimise interference from intense wind waves and typhoons on TLS observations, we primarily acquired intertidal point cloud data during the winter season (or thereafter). Three field surveys were conducted in the East Nanhui wetland in April 2018, December 2021 and December 2022. For the South Nanhui Wetland, three TLS data acquisitions were completed in January 2019, January 2021 and December 2021 (Table 1). All fieldwork conducted in this study was carried out during low tidal levels and high-visibility weather conditions to acquire higher-quality, larger-coverage TLS point clouds. During those observations, four high-reflectivity spherical targets were evenly deployed within the 60 to 100 m scanning range of the TLS monitoring

site, and RTK (Real-Time Kinematic) equipment was employed to obtain the geographic coordinates of each target. Using these coordinates, the TLS point clouds, originally in the scanner's native coordinate system, were transformed into the China Geodetic Coordinate System (CGCS2000). In addition, to quantify possible TLS errors, the elevations of 105 randomly selected sampling points were measured with a GPS-RTK system (*iRTK5*, *Hi-Target*) in the South Nanhui wetland (Fig. S1). Results show strong consistency between TLS-derived and RTK-measured elevations ($R^2 = 0.9986$, $P < 0.0001$), confirming the reliability of the TLS measurements.

The acquired high-density TLS point clouds were referenced to the same georeferencing system. Subsequently, the terrain filtering tool was applied repeatedly to remove surface protrusions, noise and other interfering elements, such as artificial breakwaters, scattered vegetation and other temporary obstacles, with the process supplemented by manual visual checks to remove residual noisy data. The terrain filtering tool primarily filters out non-ground points by defining thresholds for three parameters of the TLS point cloud data: maximum slope angle, maximum height difference and iteration distance (Fabbri *et al.*, 2017; Xie *et al.*, 2017). Finally, all processed TLS data were converted into digital elevation models (DEMs) of bare flats adjacent to salt marshes, achieving both high-precision and high-spatial resolution. We further analysed the erosion-deposition patterns and temporal changes in contours for the East and South Nanhui wetlands. Subsequently, the overlapping regions of all DEMs within both study wetlands were delineated, followed by the calculation of maximum, minimum and mean elevations. Additionally, three elevation transects were established in each study area to examine lateral geomorphological changes.

Fluvial inputs and deltaic hydrodynamics data

Annual water discharge and suspended sediment load of the Yangtze River, measured at Datong Station (Fig. 1A) between 1956 and 2022, were obtained from the Yangtze Water Resources Commission. Hourly tide level data between 2004 and 2019 were used to calculate the annual mean tidal level at Nancao station (in the South Passage) (Fig. 1B). In addition, in situ field measurements of tidal currents were collected at three fixed ship-based monitoring sites adjacent to the Nanhui Wetlands in September 2017. HXH03 Doppler current flow meters were used to measure hourly flow velocities and directions at six vertical depths. Afterwards, vertically averaged flow velocities and directions were derived from the observed tidal current data (Wang *et al.*, 2022b).

RESULTS

Changes in deltaic hydro-sediment dynamic environment

From 1950 to 2020, the water discharge supplied by the Yangtze River to its delta remained relatively stable. In contrast, the suspended sediment load showed a sustained decreasing trend following dam constructions in the basin (Fig. 2A). During Stage 1 (1956 to 1988), the average annual water discharge and sediment load were 8.67×10^{11} m^3 and 4.62×10^8 t, respectively. After the operation of the Gezhou Dam, between 1989 and 2003 (Stage 2), annual water discharge increased by 9.48% to 9.49×10^{11} m^3, while annual suspended sediment load decreased by 29.15% to 3.27×10^8 t (Fig. 2A). By contrast, during the post-implementation period of the Three Gorges Dam (2004 to 2022, Stage 3), annual water discharge increased slightly by 0.75% compared to Stage 1, while annual sediment load dropped dramatically by 73.16% to 1.24×10^8 t (Fig. 2A). Notably, due to the extreme drought in the Yangtze River Basin in 2022, the annual fluvial sediment load was only 0.67×10^8 t, its lowest level on record. In contrast, during the extreme flood years of 2016 and 2020, annual water discharge rose to 10.44×10^{11} m^3 and 11.17×10^{11} m^3, respectively, with corresponding annual suspended sediment loads of 1.52×10^8 t and 1.63×10^8 t (Fig. 2A).

At the Nancao hydrological station (Fig. 1B) in the South Passage, Yangtze Delta, the mean tidal level gradually rose at a rate of 0.62 cm year^{-1} over this period. These changes increased the inundation frequency in intertidal areas, as well as elevating the maximum and mean water levels (Fig. 2B). In addition, water samples collected during low tide conditions in the South Nanhui wetland between 2019 and 2022 indicate that intertidal SSC gradually decreased at a rate of 0.115 g l^{-1} per month (Fig. 2C). The highest value was recorded in

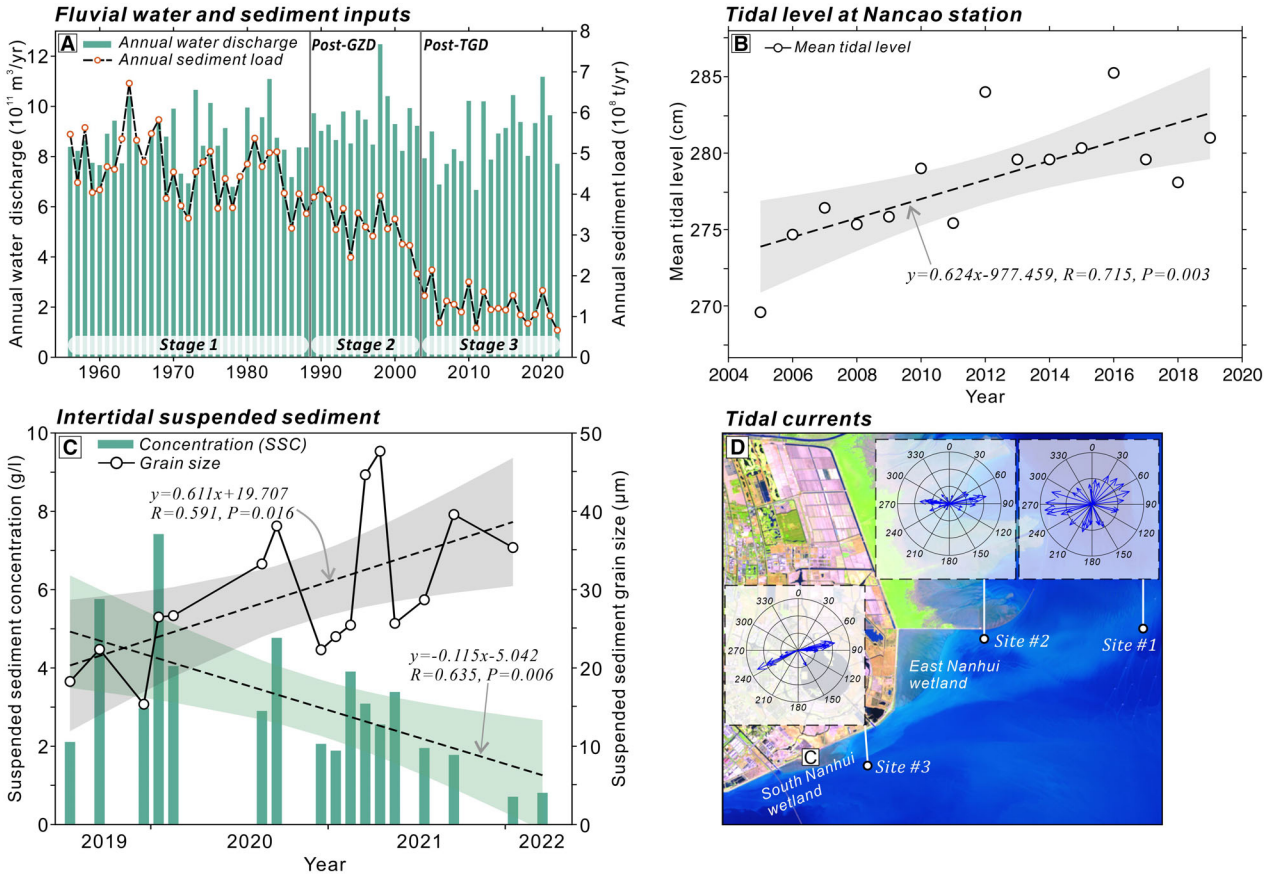

Fig. 2. (A) The annual water discharge and suspended sediment load at Datong station from 1956 to 2022, the GZD and TGD refer to the Gezhou Dam and Three Gorges Dam, respectively. (B) Changes in the annual mean tidal level at the Nancao station in the South Passage between 2005 and 2019. (C) Changes in monthly intertidal suspended sediment concentration and grain size in the South Nanhui wetland since 2019. (D) Tidal currents at three offshore sites adjacent to the Nanhui wetland.

February 2020, at 7.42 g l^{-1}, while the lowest was recorded in February 2022 at 0.70 g l^{-1}. Observations also reveal a significant coarsening trend in intertidal suspended sediment particles, and the average grain size increased from 18.27 μm in July 2019 to 35.38 μm in February 2022 (Fig. 2C). The coarsest suspended sediment grain size was observed in March 2021, rising to 47.68 μm.

Grain-size changes of intertidal surficial sediments

Along Transect E-SST in the East Nanhui wetland, intertidal sediments coarsen seaward, and grain size increased from 24.0 μm at 60 m to 52.8 μm at 900 m from the seawall, with an average grain size of 34.0 μm in November 2018 (Fig. 3A; Table 2). Surficial sediments also coarsened between October 2019 and December 2021, with mean grain size increasing from 39.9 to 41.0 μm (Table 2). During the extreme drought of the Yangtze River Basin in July 2022, bed sediments further coarsened to 60.0 μm. In December 2022, sediments in the inshore part of the transect (0 to 360 m offshore) were coarser, while finer in the mid-intertidal zones; sediment grain size coarsened again seaward, increasing from 37.9 μm at 600 m offshore to 59.8 μm at 900 m (Fig. 3A). As sediment grain size coarsened, its mean sorting coefficient decreased continuously from 1.67 in November 2018 to 1.06 in July 2022, and further declined to 0.96 in 2022 (Fig. 3B; Table 2). Moreover, sediment skewness also decreased from 2.7 in November 2018 to 0.45

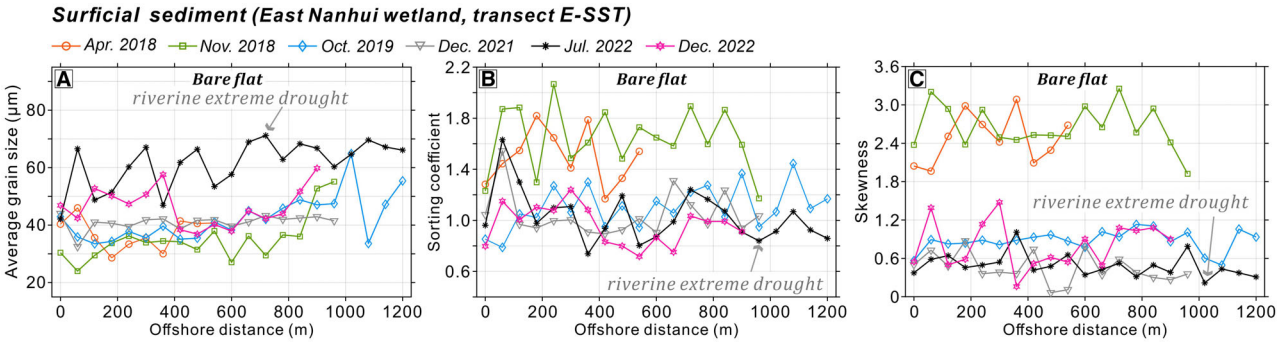

Fig. 3. Variations in the average grain size, sorting coefficient and skewness of surficial sediments along Transect E-SST in the East Nanhui wetland.

Table 2. Mean values of average grain size, sorting coefficient and skewness of surficial sediments in the East and South Nanhui wetlands.

Transect	Date	Average grain size (μm)		Sorting coefficient		Skewness	
East Nanhui wetland (E-SST)	November 2018	34.0		1.67		2.70	
	October 2019	39.9		1.09		0.89	
	December 2021	41.0		1.05		0.45	
	July 2022	60.0		1.06		0.51	
	December 2022	46.5		0.96		0.81	
South Nanhui wetland (S-SST1)	August 2018	70.5		1.39		1.00	
	January 2019	57.5		1.41		0.85	
	January 2020	57.5		1.29		1.43	
	January 2022	82.4		0.96		0.83	
	December 2022	82.7		1.16		1.38	
		Vegetated are	Unvegetated area	Vegetated area	Unvegetated area	Vegetated area	Unvegetated area
South Nanhui wetland (S-SST2)	September 2019	33.8	43.2	1.37	1.31	0.95	1.25
	January 2020	56.5	71.9	1.31	0.96	0.86	0.61
	January 2022	13.6	78.5	1.63	0.99	0.78	0.76
	August 2022	/	94.9	/	1.08	/	1.08

in December 2021, although it slightly increased to 0.81 in December 2022 (Fig. 3C; Table 2).

Sedimentary changes in the South Nanhui wetland were heterogeneous in space. In February 2018 and January 2020, the average sediment

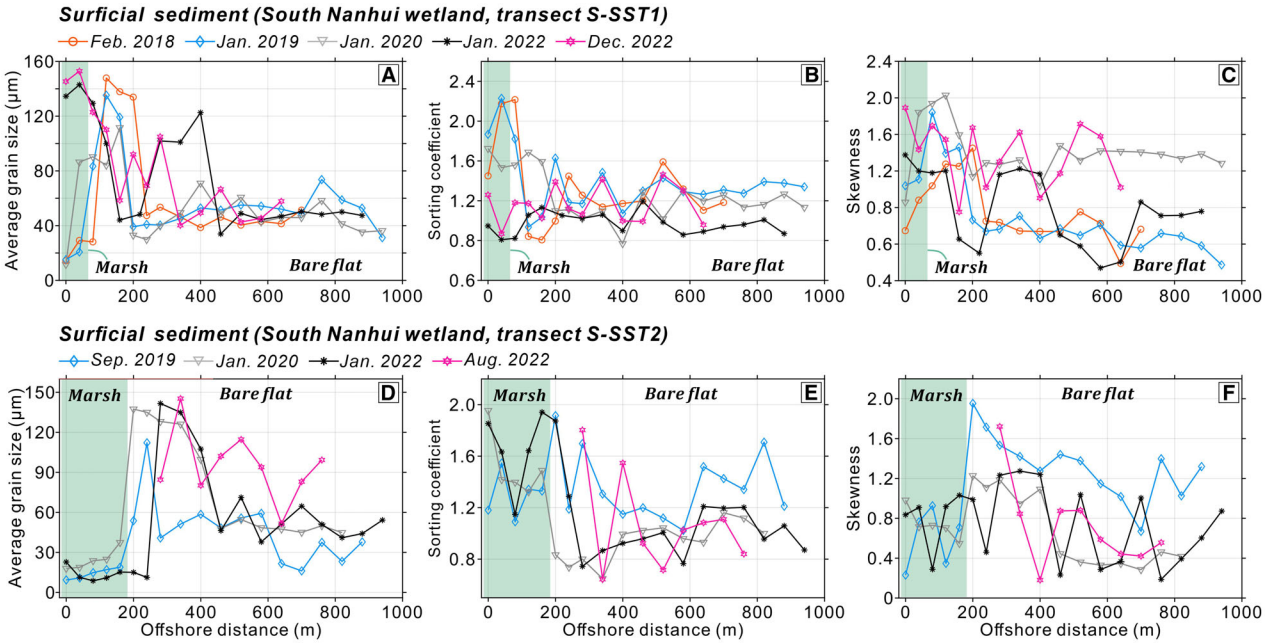

Fig. 4. Variations in the average grain size, sorting coefficient and skewness of surficial sediments along (A–C) Transects S-SST1 and (D–F) S-SST2 in the South Nanhui wetland.

grain size along the Transect S-SST1 maintained similar trends (Fig. 4A). By 2022, fine-grained sediments were replaced by coarse-grained ones in the marsh vegetated area, and more coarse-grained fractions appeared in the bare flats, especially within the range of 160 to 400 m offshore (Fig. 4A). Thus, the overall mean grain size increased from 57.5 μm in January 2020 to 82.7 μm in December 2022 (Table 2). Sediment sorting decreased with coarsening, especially at the most landward sites, and the mean value reduced from 1.39 to 1.16 during the study period (Fig. 4B; Table 2). Sediment skewness was variable, especially in sampling sites closer to the seawall, where coarse-grained sediments replaced fine-grained ones (Fig. 4C; Table 2).

Along the Transect S-SST2 in the South Nanhui wetland, surficial sediments were finer within the salt marsh vegetation; the mean sediment grain size decreased from 33.8 to 13.6 μm between September 2019 and January 2022 (Fig. 4D; Table 2). In contrast, sediment in unvegetated flats coarsened from 43.2 μm to 78.5 μm during this period. Between 2019 and 2022, the sediment sorting coefficient first decreased and then increased with coarsening grain size on the bare flat, and it increased within the salt marshes (Fig. 4E; Table 2). Sediment skewness on the bare flat also exhibited a trend of first decreasing and then increasing, with both turning points occurring in 2020 (Fig. 4F; Table 2).

Overall, the temporal coarsening trends of intertidal surficial sediment showed similar characteristics in the East and South Nanhui wetland, both accompanied by the decreasing sorting coefficient and increasing skewness (Figs 3 and 4). Meanwhile, sedimentary changes in the salt marshes of the South Nanhui wetland exhibited a fining trend, which contrasted with that on the bare flats (Fig. 4). This trend further enhanced the differentiation between vegetated and unvegetated intertidal areas.

Geomorphic erosion-deposition patterns

Sediment accumulation promoted intertidal accretion in the East Nanhui wetland. In April 2018, intertidal elevations lowered seaward and contours extended roughly parallel along the seawall (Fig. 5A, G and J). The lowest and highest elevations in the TLS observations were 0.26 m and 1.06 m, respectively, corresponding to a mean of 0.74 m (Table 3). Until December 2021, the intertidal bare flats experienced accretion; areas above 1.0 m widened eastward and

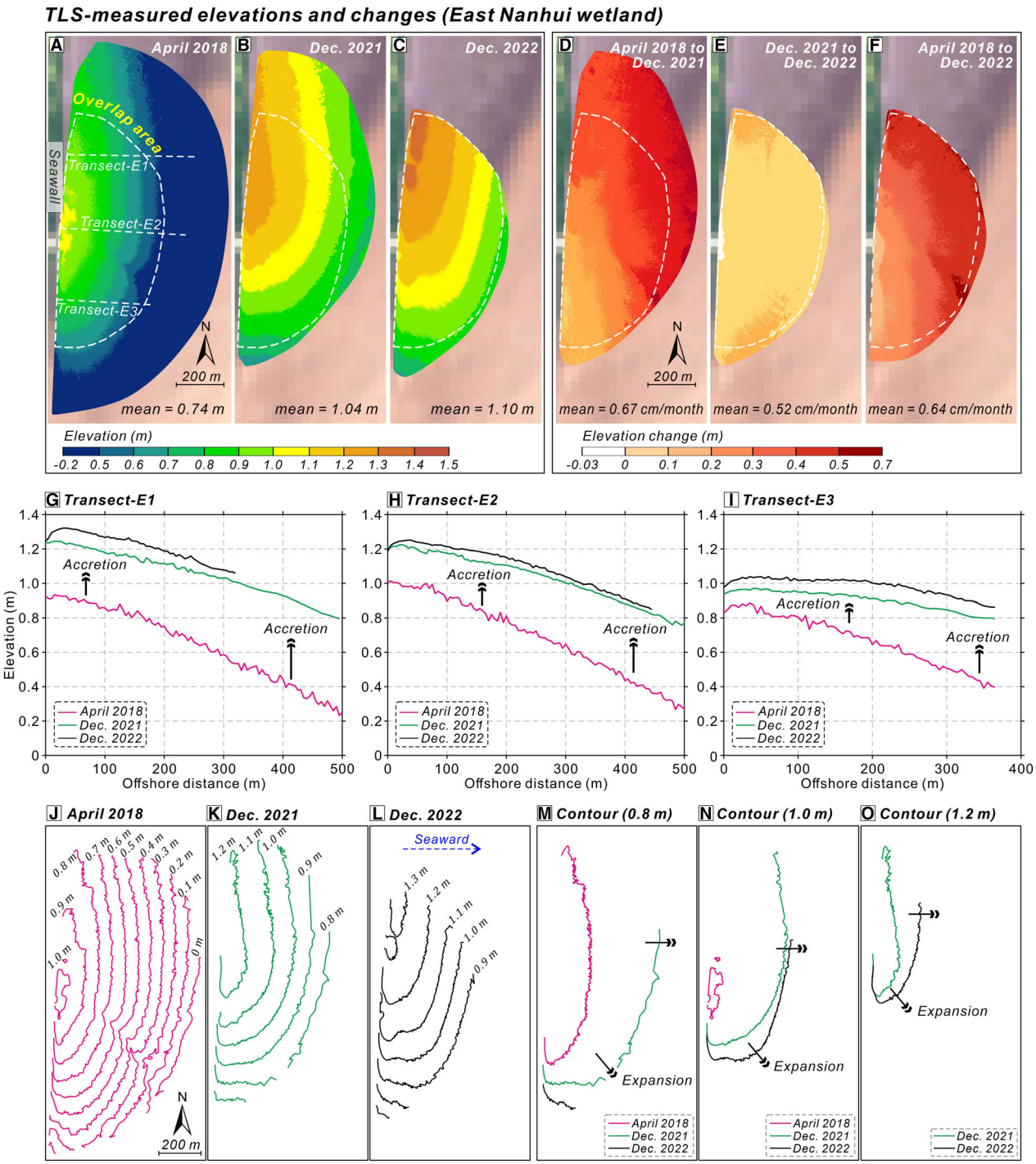

Fig. 5. (A–C) TLS-measured intertidal elevations and (D–F) erosion-deposition patterns in the East Nanhui wetland between April 2018 and December 2022. (G–I) Elevation changes along three transects (E1 to E3), and (J–O) distributions and migrations of different contours.

southeastward (Fig. 5B, D and K). Accretion was higher in the north compared to the south, where vegetated flats and areas sheltered by the groin are present (Fig. 5G to I). The mean intertidal accretion rate reached 0.67 cm month^{-1}, resulting in an increased mean elevation of 1.04 m

Table 3. The lowest, highest and mean elevations, as well as overall geomorphic change rates, in the East and South Nanhui wetlands.

Area	Date	Lowest (m)	Highest (m)	Mean (m)	Overall geomorphic change rate (cm month^{-1})
East Nanhui wetland	April 2018	0.26	1.06	0.74	0.67 (Apr. 2018 to Dec. 2021)
	December 2021	0.71	1.30	1.04	0.52 (Dec. 2021 to Dec. 2022)
	December 2022	0.76	1.48	1.10	0.64 (Apr. 2018 to Dec. 2022)
South Nanhui wetland	January 2019	−0.11	3.72	0.69	−1.05 (Jan. 2019 to Jan. 2021)
	January 2021	−0.14	2.41	0.43	−1.58 (Jan. 2021 to Dec. 2022)
	December 2022	−0.61	2.21	0.07	−1.31 (Jan. 2019 to Dec. 2022)

(Table 3). Seaward progradation rate further enhanced until December 2022, with a mean accretion rate of 0.52 cm month^{-1} between December 2021 and December 2022 (Fig. 5C, E, L to O; Table 3). Overall, the minimum elevation rose from 0.26 m to 0.76 m from April 2018 to December 2022, and the maximum elevation increased from 0.74 m to 1.10 m at the same time. The mean sedimentation rate was 0.64 cm month^{-1} (Fig. 5F, Table 3).

In the South Nanhui wetland, the bare flat area in front of the salt marsh vegetation suffered severe erosion. In January 2019, a sand bar approximately 100 m wide was present in front of the salt marsh; its elevation on the seawall side rapidly decreased from 2.4 to 0.7 m seaward (Fig. 6A, G to I). From January 2019 to January 2021, the elevation decreased by 1.0 m within the sand bar (Fig. 6A, B, and D). On the contrary, elevations of the seaward bare flats eroded slightly by 0.3 to 0.4 m (Fig. 6G to I). The steep part of the bare flat near the vegetated area retreated landward by about 40 to 60 m and experienced sediment coarsening (Fig. 6D, J, K, M to O). Meanwhile, the intertidal runnel extended westward, with an overall erosion rate of 1.05 cm month^{-1} (Table 3). From January to December 2021, erosion along the vegetated edge intensified further, triggering the retreat of the vegetated edge and net sediment loss, forming steep marsh scraps (Fig. 6C, E, M to O). Erosion was also higher in the seaward bare flats compared to the previous period (Fig. 6G to I). Therefore, intertidal elevations lowered seaward, and the net erosion rate grew to 1.58 cm month^{-1} with a mean elevation of only 0.07 m (Fig. 6F; Table 3). Overall, the net erosion rate within the observation area reached 1.31 cm month^{-1} from January 2019 to December 2022.

Dynamics of native and invasive salt marsh vegetation

Salt marsh vegetation was rapidly expanding in the whole East Nanhui wetland between 2019 and 2022. The area of native and invasive marsh species was 14.53 ha and 7.27 ha in July 2019, respectively, with a total vegetated area of 21.80 ha (Table 4). By July 2022, native *Scirpus mariqueter* expanded by 221.1%, while invasive *Spartina alterniflora* expanded by 58.5%; the total salt marsh area increased to 46.37 ha (Table 4).

Salt marshes rapidly expanded after prolonged accretion in the East Nanhui wetland. In July 2019, invasive *Spartina alterniflora* grew within the breakwater for a total area of 3.95 ha (Fig. 7A). Few native *Scirpus mariqueter* clusters developed on the seaward bare flats near the groin, for a total area of 0.057 ha (Fig. 7A; Table 4). Three years later, in July 2022, the area of *Spartina alterniflora* within the breakwater remained stable, with a 5.0% increase (Fig. 7C), whereas native and invasive marsh species outside of the breakwater rapidly spread seaward to 21.57 ha and 5.74 ha, respectively, which were 378 and 290 times larger than before (Fig. 7B; Table 4). As a result, the total vegetated area expanded 7.2 times to 31.25 ha compared to July 2022 (Table 4). Salt marsh' width increased from south to north (towards the groin), reaching 560 m, accompanied by lower fragmentation (Fig. 7B). Hence, the native *Scirpus mariqueter*, an important pioneer species in the Yangtze

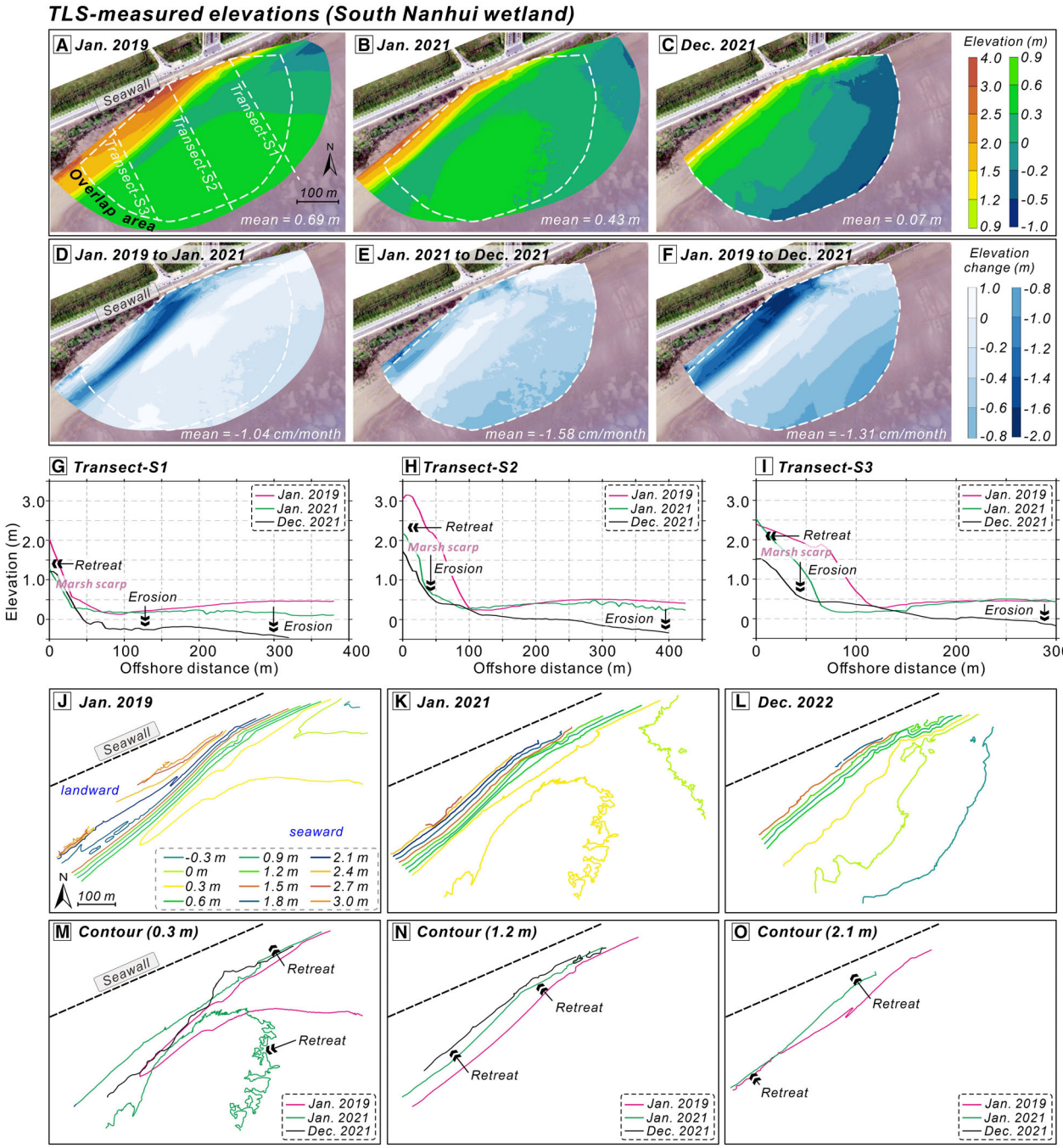

Fig. 6. (A–C) TLS-measured intertidal elevations and (D–F) erosion-deposition patterns in the South Nanhui wetland between January 2019 and December 2021. (G-I) Elevation changes along three transects (S1 to S3) and (J–O) distributions and migrations of different contours.

Delta, colonised the bare flats after the sustained accumulation of coarse sediments.

In the South Nanhui wetland, salt marshes retreated and experienced species shifts. In July 2018, salt marshes showed a predominantly seaward protruding pattern, with some scattered patches developing in their easternmost part (Fig. 8A). The native *Scirpus mariqueter* grew in seaward locations at lower elevations, totalling 15.15 ha, while

Table 4. Changes in salt marsh areas in the East and South Nanhui wetlands.

		Scirpus mariqueter		*Spartina alterniflora*		Total	
Area	Date	Area (ha)	Change	Area (ha)	Change	Area (ha)	Change
East Nanhui wetland	July 2019	0.06	/	3.76	/	3.81	/
	July 2022	21.57	37742.5%	9.68	157.8%	31.25	719.7%
South Nanhui wetland	July 2018	15.15	/	4.02	/	19.17	/
	July 2019	14.47	−4.5%	3.51	−12.6%	17.98	−6.2%
	July 2022	1.46	−89.9%	13.66	288.7%	15.12	−15.9%

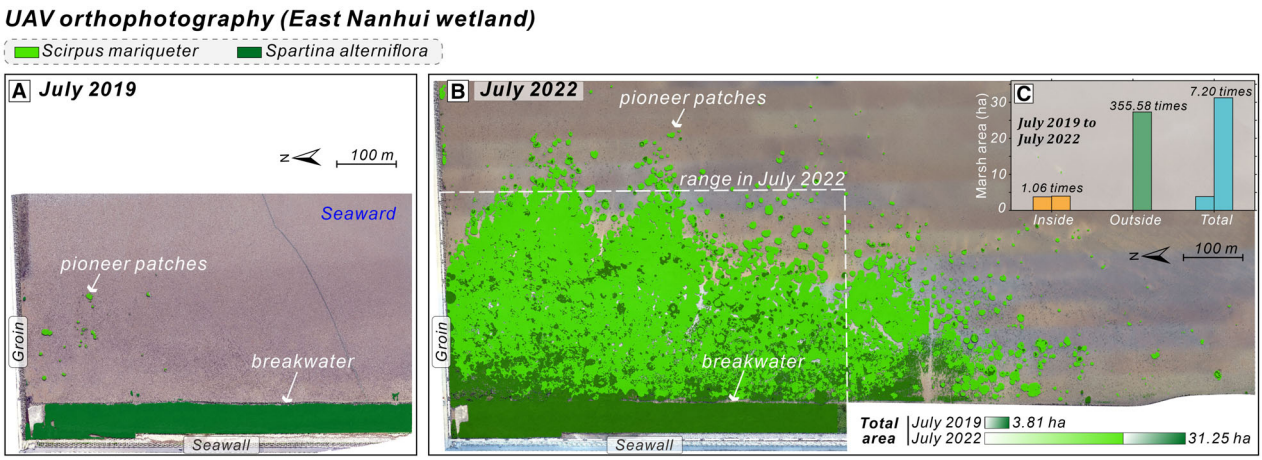

Fig. 7. UAV orthophotography and classification of salt marshes (*Scirpus mariqueter* and *Spartina alterniflora*) in the East Nanhui wetland in July 2019 and July 2022.

invasive *Spartina alterniflora* clustered closer to the seawall (primally within the breakwater) with a total area of 4.02 ha (Fig. 8A; Table 4). By July 2019, significant erosion had occurred alongside landward retreat at the central edge of the native salt marshes, resulting in fewer pioneer vegetation patches seaward, coarser-grained surficial sediments and steep marsh scarps (Fig. 8B). The total vegetated area reduced by 6.2% from 19.17 ha to 17.98 ha (Table 4). Meanwhile, *Spartina alterniflora* started to invade the intertidal area, replacing *Scirpus mariqueter*; therefore, the latter decreased by 12.6% compared to July 2018, which was higher than the former's decrease of 4.50% (Table 4). In the following 3 years, the marsh shifted dramatically, with *Spartina alterniflora* expanding seaward and trapping fine-grained sediments in July 2022, while the native *Scirpus mariqueter* remained confined in the westernmost parts, and salt marshes in the easternmost part had nearly disappeared (Fig. 8C to E). The native species area further decreased by 89.9% between July 2019 and July 2022, while the invasive species area increased by 288.7%. As a result, marshland was reduced by 15.90% to 15.12 ha (Table 4). Thus, during the UAV-based surveying period, the total area of salt marshes in the South Nanhui wetland decreased by 21.1%, while the invasive *Spartina alterniflora* expanded by 239.8%.

Compared to the East Nanhui wetland, salt marshes in the South Nanhui wetland grew along the shore and were more easily colonised by invasive species (Figs 7 and 8; Table 4). The overall vegetation cover was dominated exclusively by *Spartina alterniflora*, accompanied by the retreat of the vegetation edge and the erosion of the sediment bed (Figs 7 and 8).

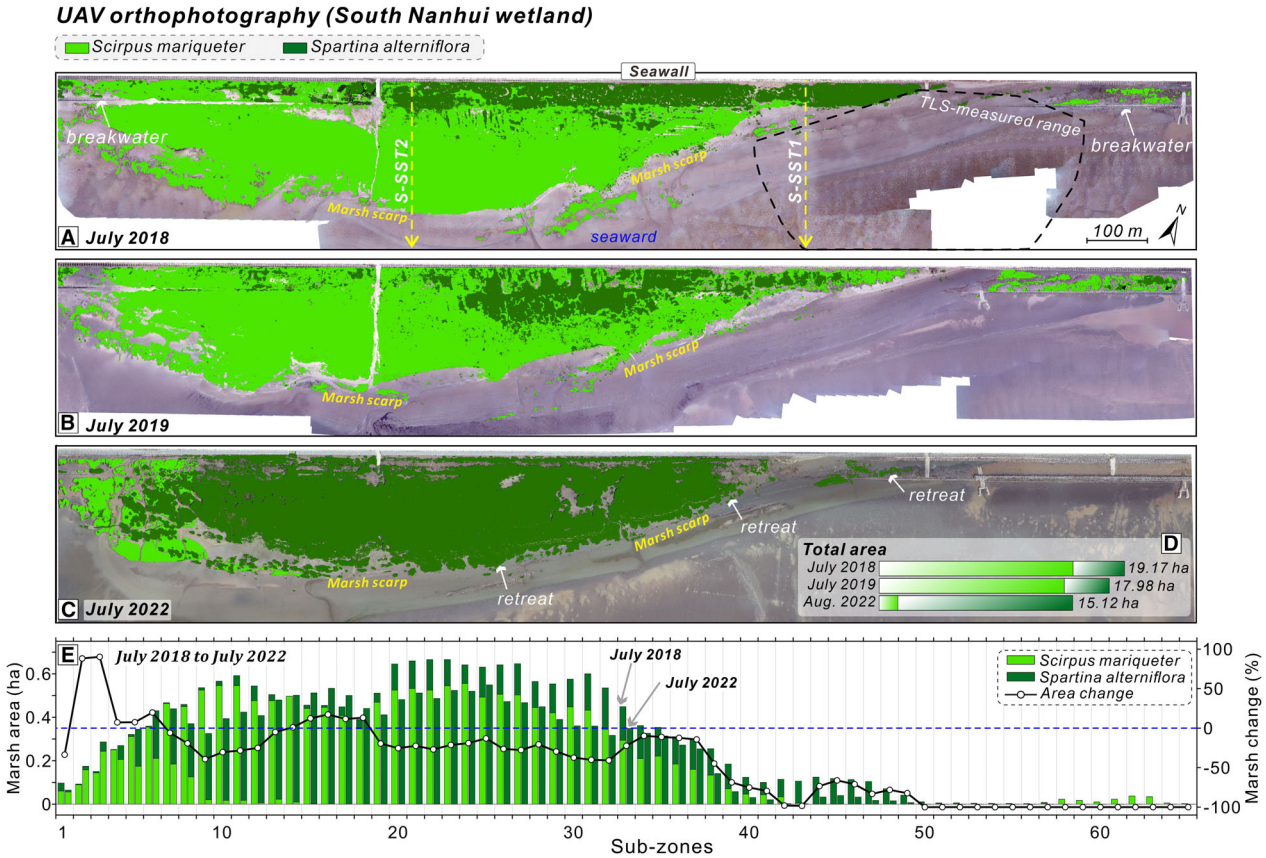

Fig. 8. (A–D) UAV orthorectified images and classification of salt marshes (*Scirpus mariqueter* and *Spartina alterniflora*), and calculation of their total area changes in the South Nanhui wetland in July 2018, July 2019 and July 2020. (E) Salt marsh area and change proportions in different alongshore sub-zones from July 2018 to July 2020.

DISCUSSION

Delta sedimentary shifts under changing external drivers

Reduced fluvial sediment inputs and SLR affect sediment budgets in deltaic wetlands. High sediment availability supports the accretion and progradation of salt marshes and bare flats, offsetting the threats of land subsidence and habitat degradation (Michener *et al.*, 1997; Fagherazzi *et al.*, 2012; Willemsen *et al.*, 2022; Zhang *et al.*, 2022). Accelerated SLR can alter hydrodynamics and sediment transport between delta channels and tidal wetlands, disturbing sediment budgets in a delta system and triggering net land loss (Schwarz *et al.*, 2016; Fagherazzi *et al.*, 2020; Nienhuis & van de Wal, 2021). In the Yangtze Delta, the fluvial sediment supply has been decreasing since the 1960s, while water discharge has remained stable (Fig. 2A; Yang *et al.*, 2011; Dai *et al.*, 2018a). Following the construction of the Three Gorges Dam, the annual riverine sediment load at Datong station decreased to 1.28×10^8 t between 2004 and 2022, 72.6% less than levels recorded in the 1960s to 1970s (Fig. 2A). Meanwhile, the SLR rate at Nancao station was 6.2 mm year^{-1} between 2005 and 2019 (Fig. 2B).

Hence, some studies have suggested that tidal dominance is increasing in the Yangtze Delta, accompanied by the declining sediment supply, causing extensive bed erosion in inner channels and tidal shoals and the landward migration of depocenter in the subaqueous front (Dai *et al.*, 2014; Mei *et al.*, 2018; Wang *et al.*, 2020; Luo *et al.*, 2023; Lou *et al.*, 2025). This study focused on the Nanhui Wetland, the largest marginal wetland in the Yangtze Delta, where intertidal eco-morphodynamics reflect these deltaic

sedimentary shifts (Fan *et al.*, 2017; Dai *et al.*, 2018b; Wang *et al.*, 2024). Based on the high-resolution interannual in situ observations using UAV and TLS technologies, this study reveals that significant transitions have occurred in the eco-morphodynamic trajectories of the East and South Nanhui wetlands between 2018 and 2022 in response to changing deltaic land-sea interactions (Figs 3 to 8). The two technologies (UAV and TLS) can effectively overcome the limitations of traditional monitoring methods, which primarily rely on sampling and/or measurements from scattered field sites, thereby providing more comprehensive and detailed evidence for the transformation of intertidal landscapes driven by natural and human influences (Mancini *et al.*, 2013; Xie *et al.*, 2017; Pinton *et al.*, 2021; van der Wal *et al.*, 2023).

In the past, the Nanhui wetland was the fastest-silting tidal flat in the Yangtze Delta, where intertidal sedimentation and salt marsh growth have favoured land building and shoreline progradation (Li, 1991; Fan *et al.*, 2017; Wang *et al.*, 2018a, 2018b; Guo *et al.*, 2021). These processes are governed by frequent water-sediment exchanges between the Nanhui wetland and the adjacent South Passage and Hangzhou Bay (Fig. 1B; Yun, 2004). The sediment transport pathways and total sediment load directly influence the availability and grain-size properties of sediments to the intertidal and subtidal areas (Chen *et al.*, 1999; Yang *et al.*, 2003; Dai *et al.*, 2008). However, the southern part of the Yangtze Delta has experienced intensive land reclamation activities since the 1980s, and a series of groins were constructed in 2015 to promote tidal flat sedimentation (Fig. 9). Consequently, due to increased input of coarse-grained sediment from the upstream and net sediment exports from the delta system, the sediment deposited in the Nanhui wetland has been experiencing continuous coarsening (Figs 3 and 4). These results are consistent with other previous findings (Wei *et al.*, 2022; Wang *et al.*, 2024). In this context, the comprehensive analyses of high-precision TLS topographic data and UAV aerial imagery elucidated that, between 2018 and 2022, the erosion-deposition patterns of the intertidal sediment bed and salt marsh dynamics exhibited significant differences between the East and South Nanhui wetlands. Specifically, this study shows that the East Nanhui wetland continued to experience accretion with the supply of coarser-grained sediment, with salt marshes expanding eastward and southeastward (Figs 5 and 7; Wang *et al.*, 2024). In contrast, the South Nanhui wetland experienced salt marsh retreat and erosion of bare flats, with coarsening of suspended and surficial sediments (Figs 2C, 6 and 8; Chen *et al.*, 1988; Yun, 2004; Wang *et al.*, 2018a; Wei *et al.*, 2020).

Similar changes are also present in other mega-deltas, where lowering fluvial sediment supply and SLR trigger systematic sedimentary shifts in salt marshes and bare flats. Riverine sediment load in the Mississippi Delta has decreased by 50%. Blum & Roberts (2009) projected that over 10 000 km^2 of additional tidal wetlands will be drowned by 2100 due to sustained land subsidence and SLR. Large-scale erosion occurred along the Mekong Delta shoreline between 2003 and 2012, particularly in the mud-dominated South China Sea coast, driven by reduced fluvial sediment input and stronger coastal hydrodynamics (Anthony *et al.*, 2015; Li *et al.*, 2017). Mild net accretion was concentrated on the sand-dominated Mekong deltaic distributary mouths. Therefore, fluctuations in fluvial sediment input are the most critical factors governing erosion and accretion in most deltas. Reduced sediment input will inevitably impact the continuous sedimentation and geomorphological stability of tidal flats and salt marshes (Fagherazzi *et al.*, 2012; Willemsen *et al.*, 2022; Day *et al.*, 2024).

In the Yellow Delta, surficial sediments in both active and abandoned delta lobes have also coarsened significantly (Liu *et al.*, 2022). However, the reasons for sediment coarsening here are distinctly different; they were driven primarily by an increase in sediment grain size resulting from the resuspension of channel bed sediments following a Water-Sediment Regulation Scheme, and by localised net erosion, respectively (Fu *et al.*, 2021; Liu *et al.*, 2022). These two sedimentary changes partially correspond with the findings in the East Nanhui wetland and South Nanhui wetland from this study, indicating that sedimentary patterns in different regions of the deltaic intertidal zones and subaqueous areas are accelerating their shifts under the combined effects of reduced overall sediment supply and inputs of coarsened sediment (Figs 3 to 6) (Chen *et al.*, 2001; Edmonds & Slingerland, 2010; Day *et al.*, 2011; Wang *et al.*, 2024). In addition, compared with other large river deltas worldwide, such sedimentary shifts in the Yangtze Delta have been more severely influenced by both historical and

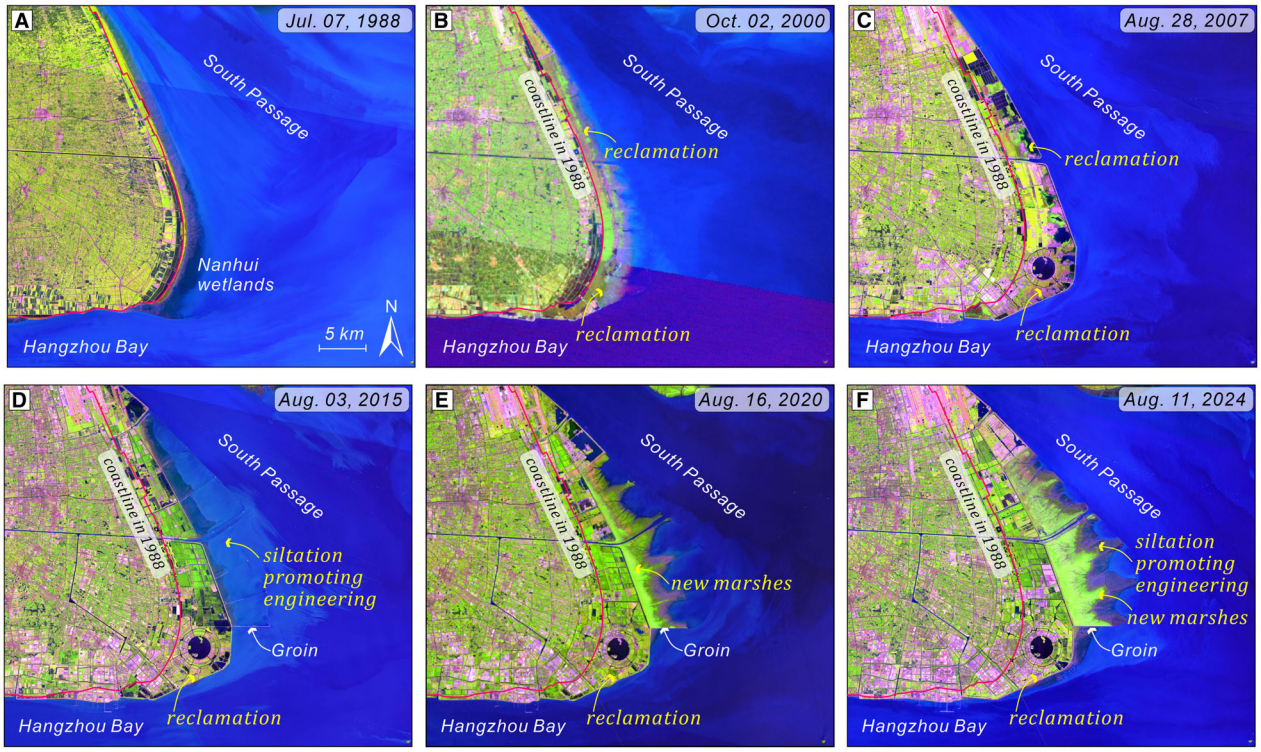

Fig. 9. Landsat satellite images showing coastal land reclamations, siltation-promoting projects and intertidal salt marsh changes in the south Yangtze Delta since 1988.

current artificial engineering structures (Syvitski & Saito, 2007; Dai *et al.*, 2008; Wang *et al.*, 2018a; Nienhuis *et al.*, 2020). Therefore, these key findings refine the prevailing understanding that annual-scale erosion in deltaic tidal flats is not solely attributed to insufficient fluvial sediment supply. Instead, engineering structures exert a pivotal role in reshaping the intertidal sedimentary processes and eco-morphodynamics within intensively human-impacted modern river deltas.

Bifurcation of intertidal eco-morphodynamic trajectories

Engineering structures induce distinct eco-morphodynamic trajectories by regulating hydrodynamic, sedimentary and vegetative interactions. To meet the growing land demand in Shanghai, a siltation-promoting project was initiated on the north side of the East Nanhui wetland in 2015 to reclaim an area of approximately 150 km^2 (Fig. 9D to F). As a result, coarse-grained sediments from the subaqueous delta have been transported by flooding tidal currents and deposited in the intertidal area sheltered by groins. Since then, native salt marsh species rapidly colonised the upper intertidal zone (Fig. 9E and F, S2; Wei *et al.*, 2019; Wang *et al.*, 2024; Wu *et al.*, 2024). Artificial groins also increased sedimentation at our site in the East Nanhui wetland (Fig. 10A to C). Field observations show that tidal currents changed from an offshore rotating pattern (Site #1) to a roughly parallel direction (Site #2) along the groin in the south of the siltation-promoting project (Fig. 2D). In general, salt marsh growth is largely dependent on intertidal elevation, inundation duration, water salinity and hydro-sediment dynamic conditions (D'Alpaos, 2011; Bádenas *et al.*, 2018; Fagherazzi *et al.*, 2020).

In the Yangtze Delta, the habitat elevation thresholds for the native *Scirpus mariqueter* and invasive *Spartina alterniflora* were 1.8 m and 2.5 m, respectively, and the latter exhibited stronger salinity resilience and ecological competitive advantage (Jiang *et al.*, 2009; Ge *et al.*, 2015). In the area sheltered by the groin in the

Fig. 10. Field photographs of the Nanhui wetlands in different sites. (A) Pioneer salt marshes in the northern siltation-promoting project in October 2017. (B,C) Scattered pioneer vegetation on bare flats in the East Nanhui wetland in October 2017 and July 2019, respectively. (D–F) Eroded bare flats, exposed salt marsh roots and eroded ponds near the seawall and breakwaters in the South Nanhui wetland in July 2019. (G) Artificially planted salt marshes for erosion prevention in the South Nanhui wetland in April 2019. (H–J) Eroded bare flats and exposed vegetation roots at the edges of salt marshes in the South Nanhui wetland in January 2022.

East Nanhui wetland, the intertidal elevation was about 1.2 to 2.7 m in 2022, with a gentle seaward slope and coarsening surficial sediment (Fig. 11A to C); hence, native pioneer marsh species began to expand and colonise the middle intertidal zone adjacent to the groins (Fig. 7). As a result, the total salt marsh area expanded by 720% to 31.25 ha from 2019 to 2022. However, the land-most marsh vegetation was replaced by invasive marsh species, because the high sedimentation rate promoted the root-system growth and seaward settlement of

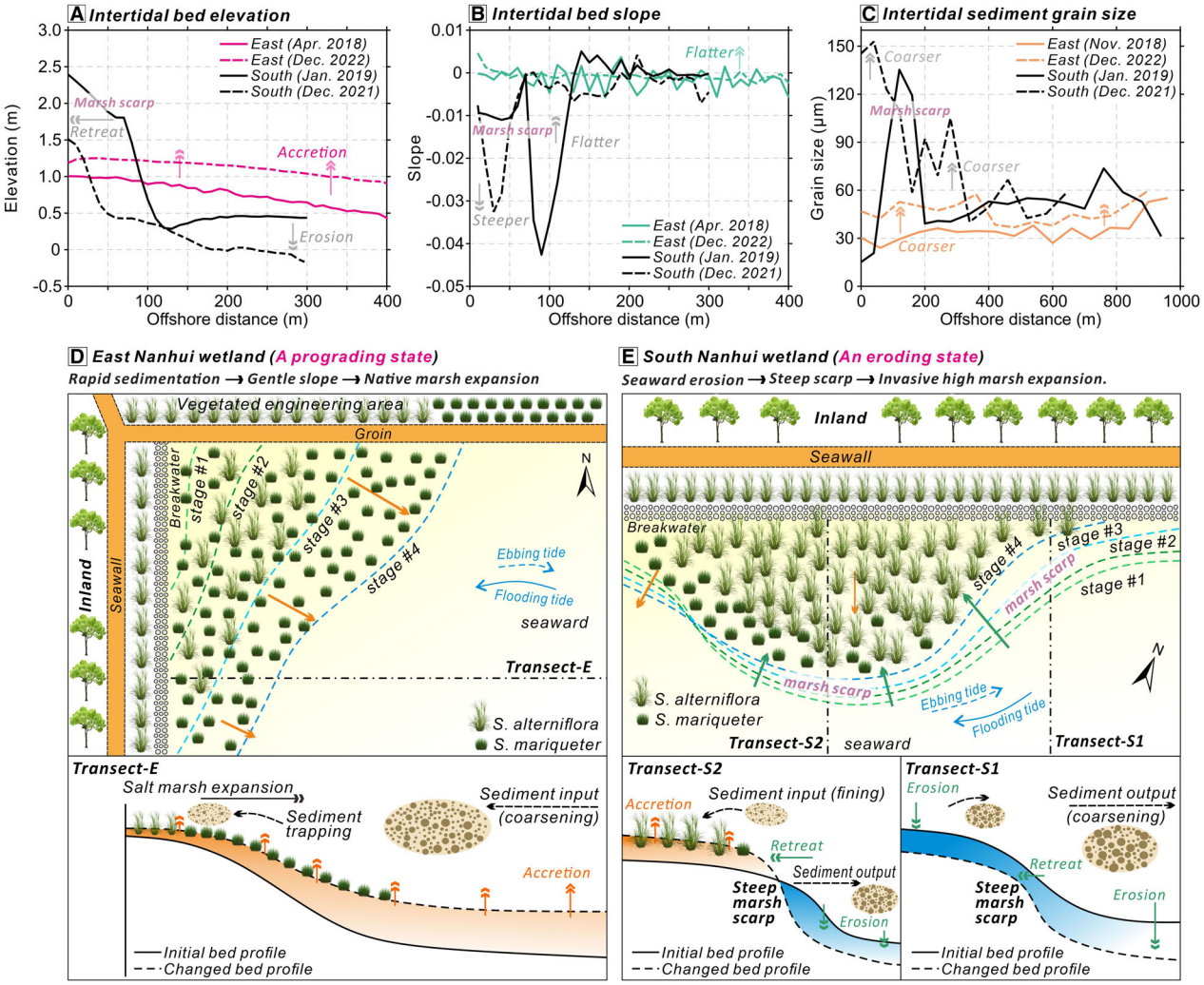

Fig. 11. The evolution of salt marshes and bare flats in the Nanhui wetlands is bifurcating into two distinct states. (A–C) Comparisons of the changes in intertidal elevation, bed slope and average sediment grain size in the East and South Nanhui wetlands during the study period. (D) Schematic diagram of the East Nanhui wetland, which is in a prograding state due to abundant sediment deposition, and thus shows gentle intertidal bed slopes and the expansion of native marshes. (E) Schematic diagram of the South Nanhui wetland, which is in an eroding state, characterised by the retreat of native marshes, the expansion of invasive salt marshes, the presence of steep marsh scarps and a reduction in low-lying areas.

Spartina alterniflora (Figs 5, 7, 10A to C, 11A to C) (He *et al.*, 2007; Li *et al.*, 2009; Zhu *et al.*, 2012; Zhou *et al.*, 2024).

Long-term monitoring of tidal marsh restoration projects in San Francisco Bay, USA, demonstrates that with high sediment input and sustained accumulation, intertidal elevation increases, eventually reaching thresholds suitable for salt marsh colonisation (Brand *et al.*, 2012). Numerical simulations from Zhang *et al.* (2022) also indicate that increased river flow can enhance intertidal sediment accumulation rates, thereby strengthening the resilience of the mudflat to erosion. Field experiments conducted in the Ems estuary, located at the border between the Netherlands and Germany, suggested that increasing sediment supply with a 25% mud fraction and introducing pioneer salt marsh species can enhance salt marsh coverage and species richness (Baptist *et al.*, 2021). This is critical to the integration of nature-based defences into the coastal ecosystem. In the East

Nanhui wetland, Yangtze Delta, high-resolution UAV imagery showed that as coarse-grained sediment continued to accumulate, salt marsh vegetation (both native and invasive species) expanded seaward at a rate of up to 200 m $year^{-1}$ (Fig. 7). This expansion was faster in the northern parts of the wetland, consistent with the spatial pattern of sedimentation thickness detected by TLS (Fig. 5). Therefore, our findings from the East Nanhui wetland clarify that siltation-promoting projects have effectively shaped a unique intertidal system characterised by the co-evolution trajectory of intertidal sedimentary processes and salt marsh ecosystems (Fig. 11D).

In contrast, land reclamation amplified salt marsh degradation in the South Nanhui wetland. The supratidal and intertidal zones were squeezed by reclamation between 1994 and 2006, and sediment mainly accumulated in the new upper intertidal zone with the encroachment of native marsh species (Fig. 9; Li *et al.*, 2010; Wang *et al.*, 2018b; Zhang *et al.*, 2020; Zhou *et al.*, 2021). Field measurements show that tidal currents run parallel to the isobaths, and nearshore tidal current velocity can exceed 1.0 m s^{-1} (Fig. 2D). These currents in conjunction with strong wind waves triggered salt marsh retreat, steepening the cross-shore profile and coarsening bed sediments (Fig. 11A to C; Tables 2 to 4; Wang *et al.*, 2018b; Wei *et al.*, 2020; Li *et al.*, 2022). During the study period, we observed exposed vegetation roots, marsh scarp and pond formation in the eastern part of the South Nanhui wetland (Fig. 10D to I). Most of the salt marsh platform was above 2.0 m in elevation, which was favourable for invasive marsh growth and the accumulation of more sediment (Fig. 11E). We also found that when the dense canopy of *Spartina alterniflora* replaced native marsh species, fine-grained sediments were trapped, enhancing sedimentation within the salt marsh platform with the eroded marsh edges (Figs 4, 6 and 8).

van der Wal & Pye (2004) reviewed the dynamics of salt marshes in the Greater Thames area, UK, over the past century, indicating that land reclamation, embankment construction (causing higher current velocities) and water level rise were the primary drivers of widespread salt marsh erosion. Along the Jiangsu coast, China, intensive reclamation activities since the 1980s have directly resulted in a dramatic reduction in the area and width of salt marshes, with expanding invasive salt marsh species (Zhang *et al.*, 2024). Meanwhile, seaward erosion has further exacerbated the retreat of salt marshes and the steepening of intertidal flats. Numerical simulations also showed that the vertical and horizontal changes in salt marshes respond differently to erosion caused by strong waves, and the marsh retreat can increase sediment availability within vegetation areas in the short term (Mariotti & Carr, 2014). In addition, the availability of salt marsh seeds is one crucial threshold for the lateral expansion of salt marsh vegetation (Hu *et al.*, 2015; van Regteren *et al.*, 2020). Adverse changes in intertidal hydrodynamic and topographic conditions may restrict the colonisation of pioneer salt marshes (Tommasini *et al.*, 2019). Hence, findings from the South Nanhui wetland confirmed that enhanced tidal currents and wave power resulting from large-scale reclamation activities have triggered rapid erosion of salt marsh edges (Fig. 11E). Such marsh vegetation retreat and the formation of steep marsh scarps have been captured by high-resolution UAV and TLS data, respectively. In particular, the destruction of the belowground marsh root systems has greatly reduced the natural recovery potential of native marsh species, whereas invasive marsh species have exhibited extensive expansion (Figs 6, 8, 10D to I).

At our site, due to the overlapping ecological niches of the two salt marsh species, the invasive *Spartina alterniflora* was able to utilise the soil nutrients more effectively to grow and encroach on the native *Scirpus mariqueter* over the 4 years of the study (Figs 7 and 8) (He *et al.*, 2007; Li *et al.*, 2009; Xue *et al.*, 2018; Shi *et al.*, 2025). High-resolution UAV and TLS technologies have high flexibility and the capacity to acquire large-scale, high-resolution data to study the rapid annual salt marsh dynamics, enabling them to significantly advance our understanding of intertidal biotic-abiotic feedbacks and salt marsh eco-morphodynamics (Yang *et al.*, 2003; Wiberg *et al.*, 2020; Curcio *et al.*, 2023). They are far superior to traditional observation methods, which are not only limited in data coverage but also highly labour-intensive, particularly in terms of the spatial coverage of data and investigation efficiency (Xie *et al.*, 2017; Agrillo *et al.*, 2023; van der Wal *et al.*, 2023).

Overall, the eco-morphodynamics system in the Nanhui wetland is bifurcating into two distinct states under changing natural and anthropogenic drivers. First, the East Nanhui wetland is in a prograding state, representing a system

with abundant sediment deposition, which is facilitated by the implementation of artificial siltation-promoting projects. In these conditions, the deltaic land progrades and creates expansive, low-lying areas that favour the encroachment of both native and invasive species (Fig. 11D). Second, the South Nanhui wetland is in an eroding state; scarps form in front of the wetland with retreating marsh edges, and the steep slopes of these scarps not only squeeze the native salt marsh area but also prevent its seaward expansion, thus leaving only the invasive high marsh species to survive (Fig. 11E). SLR could flood the invasive high marsh more often, thus promoting conditions favourable to native marsh species; however, the timescale of SLR is too slow compared to the deltaic land progradation/erosion timescale, so in the short term, the formation of the invasive high marsh is favoured (Fagherazzi *et al.*, 2012, 2020; Ge *et al.*, 2015; Wang *et al.*, 2024).

These two cases can represent the future trajectories of the intertidal eco-morphodynamics in the mega sediment-starved Yangtze Delta. Siltation-promoting engineering structures can capture more sediment for deposition in the intertidal area. Although sediment supply to the entire delta remains insufficient, the accretion of coarser-grained sediments helps form gentle intertidal flats, which further provide habitats for native marsh species (Chen *et al.*, 2001; D'Alpaos & Marani, 2016; Roner *et al.*, 2016; Willemsen *et al.*, 2022). In contrast, in sediment-deficient deltaic regions with increased hydrodynamics following land reclamation, erosion dominates. The seaward topographic profile gradually steepens, squeezing the intertidal zone and reducing the extent of low-lying areas; consequently, native marsh species lose their habitats, while accretion facilitates the invasion of *Spartina alterniflora* in existing salt marshes (Day *et al.*, 2011; Granse *et al.*, 2021; Zhang *et al.*, 2024).

Our findings highlight that sediment starvation not only hinders deltaic land expansion, but also that its sedimentary and geomorphic responses facilitate the expansion of invasive species within the high salt marshes. These shifts in species composition, consequently, impact both the ecosystem service functions of the intertidal area and nature-based protection strategies (Li *et al.*, 2009; Baptist *et al.*, 2021; Finotello *et al.*, 2023; Ning *et al.*, 2023). In other deltas similar to the Yangtze Delta, coastal artificial engineering structures have largely complicated the eco-morphodynamic feedbacks within the intertidal system, bifurcating the system towards distinct evolutionary trajectories (Friedrichs & Perry, 2001; Anderson & Smith, 2014; D'Alpaos & Marani, 2016; Day *et al.*, 2024).

Implications for vulnerable deltaic tidal wetlands

In this study, we integrated high-precision UAV and TLS technologies to quantify the bifurcated intertidal eco-morphodynamics in the Nanhui wetlands, Yangtze Delta, highlighting the combined effects of shifting deltaic regimes and human interventions (Fig. 12; Yun, 2004; Dai *et al.*, 2018a; Luo *et al.*, 2023). Some studies have also indicated that the hydro-sediment dynamics were largely altered in the East Nanhui wetland due to artificial groins, while the spatial patterns of flooding and ebbing tidal currents in the South Nanhui wetland did not change after reclamation but have become stronger (Wei *et al.*, 2019; Mei *et al.*, 2023; Wang *et al.*, 2024). Therefore, the shifting hydrodynamic environments, fluvial sediment discharge and intertidal slopes will more rapidly drive salt marshes' dynamics (Fig. 12A and B). We therefore suggest incorporating different eco-morphodynamic trajectories into current and future conservation and restoration efforts for delta wetlands. Specifically, for prograding intertidal ecosystems such as the East Nanhui Wetland, the existing hydro-sedimentary environments and sediment budgets sheltered by groins should be maintained, and the optimisation of the layout and height of engineering structures should be pursued (D'Alpaos, 2011; Fagherazzi *et al.*, 2020; Wiberg *et al.*, 2020; Chirol *et al.*, 2021). For eroding intertidal ecosystems, such as the South Nanhui wetland, targeted, proactive and integrated intervention measures are required. These include the restoration of gentle geomorphic slopes, sediment replenishment and the planting of native marsh vegetation (Gedan *et al.*, 2009; Brand *et al.*, 2012; Baptist *et al.*, 2021; Ning *et al.*, 2023; Day *et al.*, 2024). Importantly, the gain and loss of intertidal wetlands is an important part of the study on the tipping point in river deltas (van de Vijsel *et al.*, 2024). The rapid annual-scale changes and diverging evolutionary states in the Nanhui wetland, Yangtze Delta, provide critical support for predicting the tipping point of this mega fluvial-tidal delta (Fig. 12C).

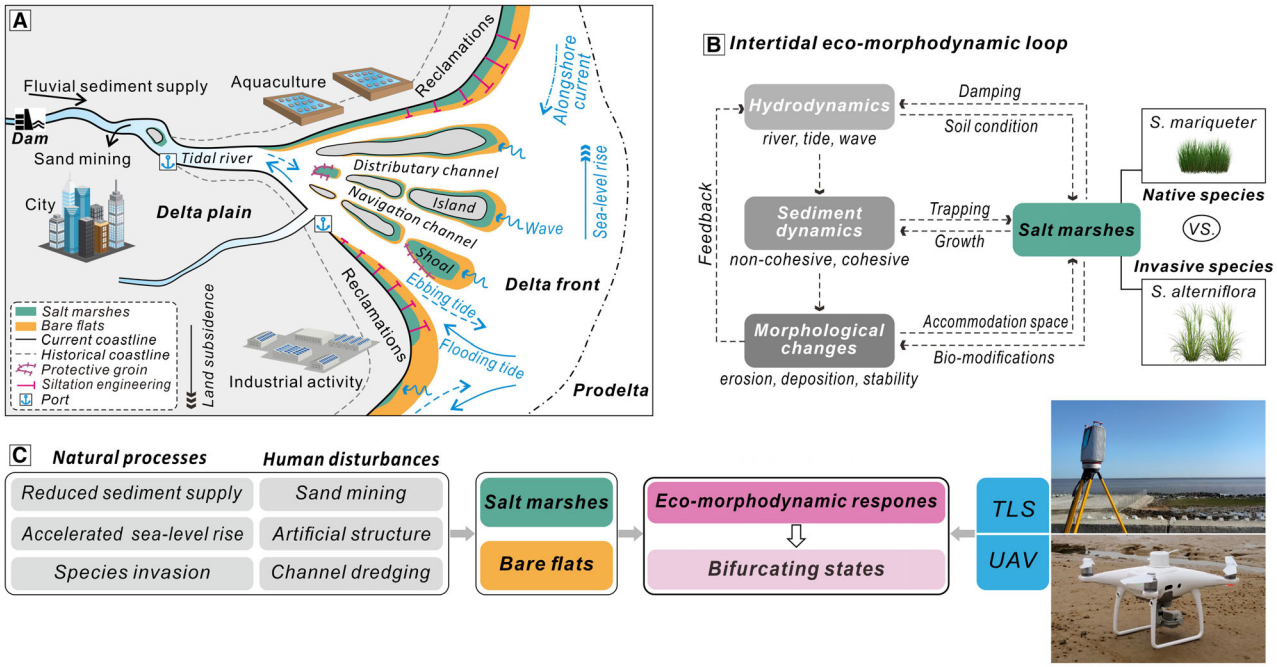

Fig. 12. (A) Conceptual diagram illustrating salt marshes, bare flats, distributary channels and anthropogenic activities in a deltaic system. (B) Intertidal eco-morphodynamic feedback loop between hydrodynamics, sediment dynamics, morphological changes and salt marsh vegetation (from Coco *et al.*, 2013). (C) The use of UAV (Unmanned Aerial Vehicle) and TLS (Terrestrial Laser Scanning) for studying the eco-morphodynamic responses of salt marshes and bare flats under natural processes and human disturbances, to further analyse their bifurcating evolutionary states.

Moreover, more quantitative studies using UAV and TLS techniques are needed to clarify the impacts of large-scale *Spartina alterniflora* clearance projects now being implemented in the Yangtze River Delta (Yang *et al.*, 2024; Wang *et al.*, 2025b). In the short term, salt marsh loss can reduce the erosion resistance and surface roughness of intertidal areas. Consequently, enhanced tidal flow velocities will induce increased sediment erosion and resuspension from the marsh substrate (Sheehan & Ellison, 2015; Wu *et al.*, 2025). However, in the medium- and long-term, the removal of invasive salt marsh species will facilitate the re-establishment and expansion of native salt marshes with suitable hydrodynamic and topographic conditions, thereby enhancing the overall sediment-trapping efficiency of the salt marsh ecosystem (Billah *et al.*, 2022; Rankin *et al.*, 2023). In the future, tidal wetland restoration and reclamation efforts should align with local sediment budgets and vegetation dynamics, leveraging eco-morphodynamic feedbacks (Blum & Roberts, 2009; FitzGerald & Hughes, 2019; Granse *et al.*, 2021). An improved dike design that incorporates the nature-based coastal protection provided by wetlands would reduce costs while helping to mitigate species invasion (Möller *et al.*, 2014; Fagherazzi *et al.*, 2020; Temmerman *et al.*, 2023; Day *et al.*, 2024).

High spatiotemporal resolution data obtained via UAV and TLS enables the analysis of variation patterns and trends in intertidal eco-morphodynamic trajectories in different scenarios, such as wetland restoration, tropical cyclone effects and salt marsh geomorphic stability. Our results highlight that fluvial/marine sediment supply and salt marsh dynamics are key factors controlling the resilience of the Yangtze delta wetlands, similar to the dynamics observed in the Mississippi, Yellow, Mekong, Ganges-Brahmaputra and Pearl deltas (Kirwan & Mudd, 2012; Nienhuis *et al.*, 2020; Campbell *et al.*, 2022). A comprehensive framework to assess the vulnerability and sustainability of salt marshes and tidal flats in modern river deltas should be developed by integrating field observations, numerical modelling and multi-source data.

CONCLUSIONS

High-resolution Unmanned Aerial Vehicle (UAV) imagery and Terrestrial Laser Scanner (TLS) topographic data were integrated in this study to examine the sedimentary and eco-morphodynamic changes in the Nanhui wetlands, the largest marginal wetland in the fluvial-tidal Yangtze (Changjiang) Delta. Our main findings are as follows:

1 Over the past six decades, the annual fluvial sediment supply from the Yangtze River has decreased by 70% (with stable water discharge) due to upstream damming, dropping to 1.23×10^4 t year^{-1} during the post-Three Gorges Dam period. The SLR rate in the Yangtze Delta reached 6.2 mm year^{-1} in the recent two decades.

2 Such induced hydrodynamic changes have overall reduced the input of fine-grained sediments to the Nanhui wetland, thus resulting in the accumulation of coarse-grained sediments under conditions of strong tidal flood dominance. The total salt marsh area rapidly increased by 113%, expanding from 21.80 ha in 2019 to 46.37 ha in 2022. During the same period, the native *Scirpus mariqueter* and invasive *Spartina alterniflora* expanded in area by 221.1% and 58.5%, respectively.

3 In the East Nanhui wetland, the siltation-promoting groins trapped more sediments, accelerating both the intertidal accumulation rate and the coarsening of surficial sediment, with better sediment sorting. Following sediment accumulation, salt marshes gradually colonised the bare flats and expanded seaward by 720%, increasing from 3.81 to 31.25 ha. The invasive *Spartina alterniflora* has encroached into the upper intertidal areas, while the native *Scirpus mariqueter* colonised the lower intertidal flats. This indicates that the intertidal eco-morphodynamics in the East Nanhui wetland are in a prograding state.

4 In the South Nanhui wetland, after coastal reclamation squeezed the intertidal zone, intensified wind waves and alongshore tidal currents have triggered salt marsh retreat and large-scale erosion of bare flat. Sediments remobilized by this erosion were deposited in the existing higher-elevation wetlands, favouring the expansion of the invasive marsh species. Additionally, erosion has produced steep scarps that separate the salt marsh from the bare flat, preventing the expansion of native marsh species. Thus, salt marshes narrowed by 15.90% between 2019 and 2022, with native salt marshes gradually replaced by invasive *Spartina alterniflora*. Thus, the intertidal eco-morphodynamics in the South Nanhui wetland are in an eroding state.

Our findings highlight that anthropogenic disturbances can significantly bifurcate the intertidal eco-morphodynamic trajectories of the mega-Yangtze Delta. Sediment scarcity not only prevents delta growth but also exacerbates the risk of exotic species invasions. A deeper understanding of how coastal artificial structures affect deltaic wetland dynamics is critical to guiding ecological restoration and implementing nature-based solutions.

ACKNOWLEDGEMENTS

The authors would like to thank Wenhong Pang, Yaying Lou, Ming Shi, Lingxiao Wang, Yuan Xiong and Jiangjie Yang of East China Normal University for their assistance in field sample collection and laboratory analysis. This study was financially supported by the National Natural Science Foundation of China (42430406, 42076174) and the Shanghai International Science and Technology Cooperation Fund Project (23230713800). S.F. was partly funded by the USA National Science Foundation awards 2224608 (PIE LTER) and 2425178 (VCR LTER). We gratefully acknowledge the anonymous reviewers and Massimiliano Ghinassi (Associate Editor) for their constructive comments and suggestions.

CONFLICT OF INTEREST

The authors declare that they have no competing financial interests or personal relationships that could have appeared to influence the work reported in this paper.

DATA AVAILABILITY STATEMENT

The data supporting the results and findings in this paper are archived in a Zenodo repository at https://zenodo.org/records/14504410, including the annual water and suspended sediment discharges of the Yangtze River, tidal levels and ranges at Nancao station and monthly

measured suspended sediment concentrations. Tidal levels were measured by the Hydrology-Water Resources Survey Bureau of the Changjiang Estuary, Changjiang Water Resources Committee. Landsat satellite imageries were downloaded publicly from the United States Geological Survey (USGS) website (https://earthexplorer.usgs.gov/). Additional detailed information that supports this study is provided in the supplementary material; further data can be obtained from the corresponding author upon reasonable request.

REFERENCES

Agrillo, E., **Filipponi, F.**, **Salvati, R.**, **Pezzarossa, A.** and **Casella, L.** (2023) Modeling approach for coastal dune habitat detection on coastal ecosystems combining very high-resolution UAV imagery and field survey. *Remote Sens. Ecol. Conserv.*, **9**, 251–267.

Allen, J.R. (2000) Morphodynamics of Holocene salt marshes: a review sketch from the Atlantic and Southern North Sea coasts of Europe. *Quatern. Sci. Rev.*, **19**, 1155–1231.

Anderson, M.E. and **Smith, J.M.** (2014) Wave attenuation by flexible, idealized salt marsh vegetation. *Coast. Eng.*, **83**, 82–92.

Anthony, E.J., **Brunier, G.**, **Besset, M.**, **Goichot, M.**, **Dussouillez, P.** and **Nguyen, V.L.** (2015) Linking rapid erosion of the Mekong River delta to human activities. *Sci. Rep.*, **5**, 14745.

Bádenas, B., **Aurell, M.** and **Gasca, J.M.** (2018) Facies model of a mixed clastic-carbonate, wave-dominated open-coast tidal flat (Tithonian-Berriasian, north-east Spain). *Sedimentology*, **65**, 1631–1666.

Baptist, M.J., **Dankers, P.**, **Cleveringa, J.**, **Sittoni, L.**, **Willemsen, P.W.J.M.**, **Van Puijenbroek, M.E.B.**, **de Vries, B.M.L.**, **Leuven, J.R.F.W.**, **Coumou, L.**, **Kramer, H.** and **Elschot, K.** (2021) Salt marsh construction as a nature-based solution in an estuarine social-ecological system. *Nat. Based Solut.*, **1**, 100005.

Billah, M.M., **Bhuiyan, M.K.A.**, **Islam, M.A.**, **Das, J.** and **Hoque, A.R.** (2022) Salt marsh restoration: an overview of techniques and success indicators. *Environ. Sci. Pollut. Res.*, **29**, 15347–15363.

Blum, M.D. and **Roberts, H.H.** (2009) Drowning of the Mississippi Delta due to insufficient sediment supply and global sea-level rise. *Nat. Geosci.*, **2**, 488–491.

Brand, L.A., **Smith, L.M.**, **Takekawa, J.Y.**, **Athearn, N.D.**, **Taylor, K.**, **Shellenbarger, G.G.**, **Schoellhamer, D.H.** and **Spenst, R.** (2012) Trajectory of early tidal marsh restoration: elevation, sedimentation and colonization of breached salt ponds in the northern San Francisco Bay. *Ecol. Eng.*, **42**, 19–29.

Calders, K., **Adams, J.**, **Armston, J.**, **Bartholomeus, H.**, **Bauwens, S.**, **Bentley, L.P.**, **Chave, J.**, **Danson, F.M.**, **Demol, M.**, **Disney, M.**, **Gaulton, R.**, **Krishna Moorthy, S.M.**, **Levick, S.R.**, **Saarinen, N.**, **Schaaf, C.**, **Stovall, A.**, **Terryn, L.**, **Wilkes, P.** and **Verbeeck, H.** (2020) Terrestrial laser scanning in forest ecology: expanding the horizon. *Remote Sens. Environ.*, **251**, 112102.

Campbell, A.D., **Fatoyinbo, L.**, **Goldberg, L.** and **Lagomasino, D.** (2022) Global hotspots of salt marsh change and carbon emissions. *Nature*, **612**, 701–706.

Changjiang Water Resources Commission (CWRC) (2023) *Changjiang River Sediment Bulletin*. Changjiang Press, Beijing. (in Chinese).

Chen, J.Y., **Shen, H.T.** and **Yun, C.X.** (1988) *Hydrodynamics and Geomorphic Evolution in the Yangtze (Changjiang) Estuary*. Shanghai Science and Technology Press, Shanghai. (in Chinese with English Abstract).

Chen, J.Y., **Li, D.J.**, **Chen, B.L.**, **Hu, F.X.**, **Zhu, H.F.** and **Liu, C.Z.** (1999) The processes of dynamic sedimentation in the Changjiang Estuary. *J. Sea Res.*, **41**, 129–140.

Chen, J.Y., **Chen, S.L.**, **Ding, P.X.** and **Yang, S.L.** (2001) Sediment transport along the Nanhui submerged spit of the Yangtze Estuary. *Resour. Environ. Yangtze Basin*, **10**, 166–172 (in Chinese with English Abstract).

Chirol, C., **Spencer, K.L.**, **Carr, S.J.**, **Möller, I.**, **Evans, B.**, **Lynch, J.**, **Brooks, H.** and **Royse, K.R.** (2021) Effect of vegetation cover and sediment type on 3D subsurface structure and shear strength in saltmarshes. *Earth Surf. Proc. Land.*, **46**, 2279–2297.

Coco, G., **Zhou, Z.**, **Van Maanen, B.**, **Olabarrieta, M.**, **Tinoco, R.** and **Townend, I.** (2013) Morphodynamics of tidal networks: advances and challenges. *Mar. Geol.*, **346**, 1–16.

Conery, I., **Brodie, K.**, **Spore, N.** and **Walsh, J.** (2020) Terrestrial LiDAR monitoring of coastal foredune evolution in managed and unmanaged systems. *Earth Surf. Proc. Land.*, **45**, 877–892.

Curcio, A.C., **Barbero, L.** and **Peralta, G.** (2023) UAV-hyperspectral imaging to estimate species distribution in salt marshes: a case study in the Cadiz Bay (SW Spain). *Remote Sens.*, **15**, 1419.

Dai, Z.J., **Chen, J.Y.** and **Lu, H.T.** (2008) Analysis on the spatial on the spatial distribution of deposition fields between the east bank and the south bank, in the Changjiang River estuary. *Trans. Oceanol. Limnol.*, **2**, 46–52 (in Chinese with English abstract).

Dai, Z.J., **Liu, J.T.**, **Wei, W.** and **Chen, J.Y.** (2014) Detection of the Three Gorges Dam influence on the Changjiang (Yangtze River) submerged delta. *Sci. Rep.*, **4**, 1–7.

Dai, Z.J., **Mei, X.F.**, **Darby, S.E.**, **Lou, Y.Y.** and **Li, W.H.** (2018a) Fluvial sediment transfer in the Changjiang (Yangtze) river-estuary depositional system. *J. Hydrol.*, **566**, 719–734.

Dai, Z.J., **Fagherazzi, S.**, **Gao, S.**, **Mei, X.F.**, **Ge, Z.P.** and **Wei, W.** (2018b) Scaling properties of estuarine beaches. *Mar. Geol.*, **404**, 130–136.

D'Alpaos, A. (2011) The mutual influence of biotic and abiotic components on the long-term ecomorphodynamic evolution of salt-marsh ecosystems. *Geomorphology*, **126**, 269–278.

D'Alpaos, A. and **Marani, M.** (2016) Reading the signatures of biologic-geomorphic feedbacks in salt-marsh landscapes. *Adv. Water Resour.*, **93**, 265–275.

Day, J.W., **Kemp, G.P.**, **Reed, D.J.**, **Cahoon, D.R.**, **Boumans, R.M.**, **Suhayda, J.M.** and **Gambrell, R.** (2011) Vegetation death and rapid loss of surface elevation in two contrasting Mississippi delta salt marshes: the role of sedimentation, autocompaction and sea-level rise. *Ecol. Eng.*, **37**, 229–240.

Day, J., **Anthony, E.**, **Costanza, R.**, **Edmonds, D.**, **Gunn, J.**, **Hopkinson, C.**, **Mann, M.**, **Morris, J.**, **Osland, M.**, **Quirk, T.**, **Rovai, A.**, **Rybczyk, J.**, **Spencer, T.**, **Stephens, J.**,

Syvitski, J., **Twilley, R.**, **Visser, J.** and **White, J.R.** (2024) Coastal wetlands in the Anthropocene. *Annu. Rev. Env. Resour.*, **49**, 105–135.

Edmonds, D.A. and **Slingerland, R.L.** (2010) Significant effect of sediment cohesion on delta morphology. *Nat. Geosci.*, **3**, 105–109.

Ensign, S.H., **Halls, J.N.** and **Peck, E.K.** (2023) Watershed sediment cannot offset sea level rise in most US tidal wetlands. *Science*, **382**, 1191–1195.

Fabbri, S., **Giambastiani, B.M.**, **Sistilli, F.**, **Scarelli, F.** and **Gabbianelli, G.** (2017) Geomorphological analysis and classification of foredune ridges based Terrestrial Laser Scanning (TLS) technology. *Geomorphology*, **295**, 436–451.

Fagherazzi, S., **Kirwan, M.L.**, **Mudd, S.M.**, **Guntenspergen, G.R.**, **Temmerman, S.**, **D'Alpaos, A.**, **Koppel, J.V.D.**, **Rybczyk, J.M.**, **Reyes, E.**, **Craft, C.** and **Clough, J.** (2012) Numerical models of salt marsh evolution: ecological, geomorphic, and climatic factors. *Rev. Geophys.*, **50**, 359.

Fagherazzi, S., **Mariotti, G.**, **Leonardi, N.**, **Canestrelli, A.**, **Nardin, W.** and **Kearney, W.S.** (2020) Salt marsh dynamics in a period of accelerated sea level rise. *Case Rep. Med.*, **125**, e2019JF005200.

Fan, D.D., **Wu, Y.J.**, **Zhang, Y.**, **Burr, G.**, **Huo, M.** and **Li, J.** (2017) South Flank of the Yangtze Delta: past, present, and future. *Mar. Geol.*, **392**, 78–93.

Finotello, A., **Tognin, D.**, **Carniello, L.**, **Ghinassi, M.**, **Bertuzzo, E.** and **D'Alpaos, A.** (2023) Hydrodynamic feedbacks of salt-marsh loss in the shallow microtidal back-barrier lagoon of Venice (Italy). *Water Resour. Res.*, **59**, e2022WR032881.

FitzGerald, D.M. and **Hughes, Z.** (2019) Marsh processes and their response to climate change and sea-level rise. *Annu. Rev. Earth Planet. Sci.*, **47**, 481–517.

Friedrichs, C.T. and **Perry, J.E.** (2001) Tidal salt marsh morphodynamics: a synthesis. *J. Coast. Res.*, **1**, 7–37.

Fu, Y., **Chen, S.**, **Ji, H.**, **Fan, Y.** and **Li, P.** (2021) The modern Yellow River Delta in transition: causes and implications. *Mar. Geol.*, **436**, 106476.

Ge, Z.M., **Cao, H.B.**, **Cui, L.F.**, **Zhao, B.** and **Zhang, L.Q.** (2015) Future vegetation patterns and primary production in the coastal wetlands of East China under sea level rise, sediment reduction, and saltwater intrusion. *J. Geophys. Res. Biogeosci.*, **120**, 1923–1940.

Gedan, K.B., **Silliman, B.R.** and **Bertness, M.D.** (2009) Centuries of human-driven change in salt marsh ecosystems. *Ann. Rev. Mar. Sci.*, **1**, 117–141.

Ghinassi, M., **D'Alpaos, A.**, **Gasparotto, A.**, **Carniello, L.**, **Brivio, L.**, **Finotello, A.**, **Roner, M.**, **Franceschinis, E.**, **Realdon, N.**, **Howes, N.** and **Cantelli, A.** (2018) Morphodynamic evolution and stratal architecture of translating tidal point bars: inferences from the northern Venice Lagoon (Italy). *Sedimentology*, **65**, 1354–1377.

Granse, D., **Suchrow, S.** and **Jensen, K.** (2021) Long-term invasion dynamics of Spartina increase vegetation diversity and geomorphological resistance of salt marshes against sea level rise. *Biol. Invasions*, **23**, 871–883.

Guo, L.C., **Zhu, C.Y.**, **Xie, W.M.**, **Xu, F.**, **Wu, H.**, **Wan, Y.Y.**, **Wang, Z.H.**, **Zhang, W.G.**, **Shen, J.**, **Wang, Z.B.** and **He, Q.** (2021) Changjiang Delta in the Anthropocene: Multi-scale hydro-morphodynamics and management challenges. *Earth Sci. Rev.*, **223**, 103850.

He, W., **Feagin, R.**, **Lu, J.**, **Liu, W.**, **Yan, Q.** and **Xie, Z.** (2007) Impacts of introduced *Spartina alterniflora* along an elevation gradient at the Jiuduansha Shoals in the Yangtze Estuary, suburban Shanghai, China. *Ecol. Eng.*, **29**, 245–248.

Hori, K., **Saito, Y.**, **Zhao, Q.**, **Cheng, X.**, **Wang, P.**, **Sato, Y.** and **Li, C.** (2001) Sedimentary facies and Holocene progradation rates of the Changjiang (Yangtze) delta, China. *Geomorphology*, **41**(2–3), 248.

Hu, Z., **Van Belzen, J.**, **Van Der Wal, D.**, **Balke, T.**, **Wang, Z.B.**, **Stive, M.** and **Bouma, T.J.** (2015) Windows of opportunity for salt marsh vegetation establishment on bare tidal flats: the importance of temporal and spatial variability in hydrodynamic forcing. *J. Geophys. Res. Biogeosci.*, **120**, 1450–1469.

Huang, H. and **Zhang, L.** (2007) A study of the population dynamics of *Spartina alterniflora* at Jiuduansha shoals, Shanghai, China. *Ecol. Eng.*, **29**, 164–172.

Jiang, L.F., **Luo, Y.Q.**, **Chen, J.K.** and **Li, B.** (2009) Ecophysiological characteristics of invasive *Spartina alterniflora* and native species in salt marshes of Yangtze River estuary, China. *Estuar. Coast. Shelf Sci.*, **81**, 74–82.

Kirwan, M.L. and **Megonigal, J.P.** (2013) Tidal wetland stability in the face of human impacts and sea-level rise. *Nature*, **504**, 53–60.

Kirwan, M.L. and **Mudd, S.M.** (2012) Response of salt-marsh carbon accumulation to climate change. *Nature*, **489**, 550–553.

Li, J.F. (1991) The rule of sediment transport on the Nanhui tidal flat in the Changjiang Estuary. *Acta Oceanol. Sinica*, **1**, 117–127.

Li, B., **Liao, C.**, **Zhang, X.**, **Chen, H.**, **Wang, Q.**, **Chen, Z.**, **Gan, Z.**, **Wu, J.**, **Zhao, B.**, **Ma, Z.**, **Cheng, X.**, **Jiang, L.** and **Chen, J.** (2009) *Spartina alterniflora* invasions in the Yangtze River estuary, China: an overview of current status and ecosystem effects. *Ecol. Eng.*, **35**, 511–520.

Li, J.F., **Dai, Z.J.**, **Liu, X.C.**, **Zhao, J.C.** and **Feng, L.X.** (2010) Research on the movement of water and suspended sediment and sedimentation in Nanhui spit of the Yangtze Estuary before and after the construction of the reclamation projects on the tidal flat. *J. Sed. Res.*, **3**, 31–37 (in Chinese with English Abstract).

Li, X., **Liu, J.P.**, **Saito, Y.** and **Nguyen, V.L.** (2017) Recent evolution of the Mekong Delta and the impacts of dams. *Earth Sci. Rev.*, **175**, 1–17.

Li, G.R., **Gong, G.N.**, **Zhang, S.L.**, **Gao, M.H.**, **Zhang, B.L.**, **Ma, Y.X.**, **He, P.M.** and **Fang, S.B.** (2022) Observation of physical variables of coastal wetland and response of wetland system under the influence of typhoon process. *Haiyang Xuebao*, **44**, 116–125.

Li, G.D., **Törnqvist, T.E.** and **Dangendorf, S.** (2024) Real-world time-travel experiment shows ecosystem collapse due to anthropogenic climate change. *Nat. Commun.*, **15**, 1226.

Liang, X.X., **Dai, Z.J.**, **Huang, H.**, **Wang, J.**, **Li, S.S.**, **Wang, R.M.** and **Pang, W.H.** (2024) Elevation inversion of mangrove tidal flat geomorphology based on UAV aerial survey. *Adv. Mar. Sci.*, **42**, 384–399 (in Chinese with English abstract).

Liu, L., **Wang, H.**, **Yang, Z.**, **Fan, Y.**, **Wu, X.**, **Hu, L.** and **Bi, N.** (2022) Coarsening of sediments from the Huanghe (Yellow River) delta-coast and its environmental implications. *Geomorphology*, **401**, 108105.

Lou, Y., **Wang, J.**, **Dong, H.**, **Yang, J.** and **Shi, H.** (2025) Dynamics, vulnerabilities, and adaptive strategies for tidal flat sustainability in a mega fluvial-tidal estuary. *Ocean Coast. Manag.*, **270**, 107916.

Luan, H.L., **Ding, P.X.**, **Wang, Z.B.** and **Ge, J.Z.** (2017) Process-based morphodynamic modeling of the Yangtze Estuary at a decadal timescale: Controls on estuarine evolution and future trends. *Geomorphology*, **290**, 347–364.

Luo, J.J., **Dai, Z.J.**, **Wang, J.**, **Lou, Y.Y.**, **Zhou, X.Y.** and **Tang, R.N.** (2023) Effects of human-induced riverine sediment transfer on deposition-erosion in the South Passage of the Changjiang (Yangtze) delta. *J. Hydrol.*, **622**, 129714.

Mancini, F., **Dubbini, M.**, **Gattelli, M.**, **Stecchi, F.**, **Fabbri, S.** and **Gabbianelli, G.** (2013) Using unmanned aerial vehicles (UAV) for high-resolution reconstruction of topography: the structure from motion approach on coastal environments. *Remote Sens.*, **5**, 6880–6898.

van Maren, D.S., **Schrijvershof, R.A.**, **Beemster, J.**, **Zhu, C.**, **Xie, D.**, **Zhou, Z.**, **Colina Alonso, A.** and **Hoitink, A.J.F.** (2025) Land reclamation impacts on tidal landscape evolution. *Rev. Geophys.*, **63**, e2024RG000860.

Mariotti, G. and **Carr, J.** (2014) Dual role of salt marsh retreat: long-term loss and short-term resilience. *Water Resour. Res.,* **50**, 2963–2974.

McManus, J. (1988) Grain size determination and interpretation. In: *Techniques in Sedimentology* (Ed Tucker, M.), pp. 63–85. Blackwell Scientific Publications, Oxford.

Mei, X.F., **Dai, Z.J.**, **Wei, W.**, **Li, W.H.**, **Wang, J.** and **Sheng, H.** (2018) Secular bathymetric variations of the North Channel in the Changjiang (Yangtze) Estuary, China, 1880–2013: causes and effects. *Geomorphology*, **303**, 30–40.

Mei, X.F., **Leonardi, N.**, **Dai, J.X.** and **Wang, J.** (2023) Cellular automata to understand the prograding limit of deltaic tidal flat. *Eng. Appl. Comput. Fluid Mech.*, **17**, 2234038.

Michener, W.K., **Blood, E.R.**, **Bildstein, K.L.**, **Brinson, M.M.** and **Gardner, L.R.** (1997) Climate change, hurricanes and tropical storms, and rising sea level in coastal wetlands. *Ecol. Appl.*, **7**, 770–801.

Möller, I., **Kudella, M.**, **Rupprecht, F.**, **Spencer, T.**, **Paul, M.**, **van Wesenbeeck, B.K.**, **Wolters, G.**, **Jensen, K.**, **Bouma, T.J.**, **Miranda-Lange, M.** and **Schimmels, S.** (2014) Wave attenuation over coastal salt marshes under storm surge conditions. *Nat. Geosci.*, **7**, 727–731.

Murray, N.J., **Phinn, S.R.**, **DeWitt, M.**, **Ferrari, R.**, **Johnston, R.**, **Lyons, M.B.**, **Clinton, N.**, **Thau, D.** and **Fuller, R.A.** (2019) The global distribution and trajectory of tidal flats. *Nature*, **565**, 222–225.

Nienhuis, J.H. and **van de Wal, R.S.** (2021) Projections of global delta land loss from sea-level rise in the 21st century. *Geophys. Res. Lett.*, **48**, e2021GL093368.

Nienhuis, J.H., **Ashton, A.D.**, **Edmonds, D.A.**, **Hoitink, A.J.F.**, **Kettner, A.J.**, **Rowland, J.C.** and **Törnqvist, T.E.** (2020) Global-scale human impact on delta morphology has led to net land area gain. *Nature*, **577**, 514–518.

Ning, Z., **Chen, C.**, **Xie, T.**, **Li, S.**, **Zhu, Z.**, **Wang, Q.**, **Cai, Y.**, **Bai, J.** and **Cui, B.** (2023) Invasive plant indirectly affects its self-expansion and native species via bio-geomorphic feedbacks: implications for salt marsh restoration. *Catena*, **226**, 107056.

Phillips, J.D. (2018) Coastal wetlands, sea level, and the dimensions of geomorphic resilience. *Geomorphology*, **305**, 173–184.

Pinton, D., **Canestrelli, A.**, **Wilkinson, B.**, **Ifju, P.** and **Ortega, A.** (2021) Estimating ground elevation and vegetation characteristics in coastal salt marshes using UAV-based LiDAR and digital aerial photogrammetry. *Remote Sens.*, **13**, 4506.

Rankin, C., **Gaston, T.**, **Sadat-Noori, M.**, **Glamore, W.**, **Morton, J.** and **Chalmers, A.** (2023) Innovative tidal control successfully promotes saltmarsh restoration. *Restor. Ecol.*, **31**, e13774.

van Regteren, M., **Amptmeijer, D.**, **De Groot, A.V.**, **Baptist, M.J.** and **Elschot, K.** (2020) Where does the salt marsh start? Field-based evidence for the lack of a transitional area between a gradually sloping intertidal flat and salt marsh. *Estuar. Coast. Shelf Sci.*, **243**, 106909.

Roner, M., **D'Alpaos, A.**, **Ghinassi, M.**, **Marani, M.**, **Silvestri, S.**, **Franceschinis, E.** and **Realdon, N.** (2016) Spatial variation of salt-marsh organic and inorganic deposition and organic carbon accumulation: Inferences from the Venice lagoon, Italy. *Adv. Water Resour.*, **93**, 276–287.

Schuerch, M., **Spencer, T.** and **Evans, B.** (2019) Coupling between tidal mudflats and salt marshes affects marsh morphology. *Mar. Geol.*, **412**, 95–106.

Schwarz, C., **Ysebaert, T.**, **Vandenbruwaene, W.**, **Temmerman, S.**, **Zhang, L.** and **Herman, P.M.** (2016) On the potential of plant species invasion influencing bio-geomorphologic landscape formation in salt marshes. *Earth Surf. Proc. Land.*, **41**, 2047–2057.

Sheehan, M.R. and **Ellison, J.C.** (2015) Tidal marsh erosion and accretion trends following invasive species removal, Tamar Estuary, Tasmania. *Estuar. Coast. Shelf Sci.*, **164**, 46–55.

Shi, M., **Dai, Z.**, **Luo, J.**, **Wang, J.**, **Pang, W.**, **Liang, X.** and **Cheng, J.** (2025) Wave attenuation over a Scirpus mariqueter salt marsh during typhoon Muifa. *Estuar. Coast. Shelf Sci.*, **315**, 109155.

Silvestri, S., **Defina, A.** and **Marani, M.** (2005) Tidal regime, salinity and salt marsh plant zonation. *Estuar. Coast. Shelf Sci.*, **62**, 119–130.

Spencer, T., **Schuerch, M.**, **Nicholls, R.J.**, **Hinkel, J.**, **Lincke, D.**, **Vafeidis, A.T.**, **Reef, R.**, **McFadden, L.** and **Brown, S.** (2016) Global coastal wetland change under sea-level rise and related stresses: the DIVA Wetland Change Model. *Global Planet. Change*, **139**, 15–30.

Syvitski, J.P. and **Saito, Y.** (2007) Morphodynamics of deltas under the influence of humans. *Global Planet. Change*, **57**, 261–282.

Syvitski, J., **Ángel, J.R.**, **Saito, Y.**, **Overeem, I.**, **Vörösmarty, C.J.**, **Wang, H.** and **Olago, D.** (2022) Earth's sediment cycle during the Anthropocene. *Nat. Rev. Earth Environ.*, **3**, 179–196.

Temmerman, S., **Horstman, E.M.**, **Krauss, K.W.**, **Mullarney, J.C.**, **Pelckmans, I.** and **Schoutens, K.** (2023) Marshes and mangroves as nature-based coastal storm buffers. *Ann. Rev. Mar. Sci.*, **15**, 95–118.

Tommasini, L., **Carniello, L.**, **Ghinassi, M.**, **Roner, M.** and **D'Alpaos, A.** (2019) Changes in the wind-wave field and related salt-marsh lateral erosion: inferences from the evolution of the Venice Lagoon in the last four centuries. *Earth Surf. Proc. Land.*, **44**, 1633–1646.

Tong, X., **Liu, X.**, **Chen, P.**, **Liu, S.**, **Luan, K.**, **Li, L.**, **Liu, S.**, **Liu, X.**, **Xie, H.**, **Jin, Y.** and **Hong, Z.** (2015) Integration of UAV-based photogrammetry and terrestrial laser scanning for the three-dimensional mapping and monitoring of open-pit mine areas. *Remote Sens.*, **7**, 6635–6662.

Törnqvist, T.E., **Cahoon, D.R.**, **Morris, J.T.** and **Day, J.W.** (2021) Coastal wetland resilience, accelerated sea-level rise, and the importance of timescale. *AGU Adv.*, **2**, e2020AV000334.

van de Vijsel, R.C., **Scheffer, M.** and **Hoitink, A.J.** (2024) Tipping points in river deltas. *Nat. Rev. Earth Environ.*, **5**, 843–858.

van der Wal, D. and **Pye, K.** (2004) Patterns, rates and possible causes of saltmarsh erosion in the Greater Thames area (UK). *Geomorphology*, **61**, 373–391.

van der Wal, D., **van Dalen, J.**, **Willemsen, P.W.**, **Borsje, B.W.** and **Bouma, T.J.** (2023) Gradual versus episodic lateral saltmarsh cliff erosion: evidence from Terrestrial Laser Scans (TLS) and Surface Elevation Dynamics (SED) sensors. *Geomorphology*, **426**, 108590.

Wang, Z., **Saito, Y.**, **Zhan, Q.**, **Nian, X.**, **Pan, D.**, **Wang, L.**, **Chen, T.**, **Xie, J.L.**, **Li, X.** and **Jiang, X.** (2018a) Three-dimensional evolution of the Yangtze River mouth, China during the Holocene: impacts of sea level, climate and human activity. *Earth Sci. Rev.*, **185**, 938–955.

Wang, J., **Dai, Z.J.**, **Wei, W.**, **Ge, Z.P.**, **Pang, W.H.**, **Ma, B.B.**, **Mei, X.F.** and **Yu, Y.W.** (2018b) LiDAR-based recent morphodynamic study of south Nanhui tidal flat, Changjiang Estuary. *Oceanol. Limnol. Sinica*, **49**, 756–768 (in Chinese with English Abstract).

Wang, J., **Dai, Z.J.**, **Mei, X.F.** and **Fagherazzi, S.** (2020) Tropical cyclones significantly alleviate mega-deltaic erosion induced by high riverine flow. *Geophys. Res. Lett.*, **47**, e2020GL089065.

Wang, J., **Dai, Z.J.**, **Fagherazzi, S.** and **Long, C.Q.** (2022a) A novel approach to discriminate sedimentary characteristics of deltaic tidal flats with terrestrial laser scanner: results from a case study. *Sedimentology*, **69**, 1626–1648.

Wang, J., **Dai, Z.J.**, **Fagherazzi, S.**, **Zhang, X.H.** and **Liu, X.Q.** (2022b) Hydro-morphodynamics triggered by extreme riverine floods in a mega fluvial-tidal delta. *Sci. Total Environ.*, **809**, 152076.

Wang, J., **Dai, Z.J.**, **Fagherazzi, S.**, **Lou, Y.Y.**, **Mei, X.F.** and **Ma, B.B.** (2024) Large-scale sedimentary shift induced by a mega-dam in deltaic flats. *Sedimentology*, **71**, 1084–1112.

Wang, J., **Dai, Z.J.**, **Mei, X.F.**, **Duan, H.F.** and **Nienhuis, J.H.** (2025a) Response time of global deltas to changes in fluvial sediment supply. *Nat. Commun.*, **16**, 5573.

Wang, D., **Labra, F.A.**, **Yang, H.**, **Hu, Y.**, **Zhao, Z.**, **Zhou, W.** and **Yuan, L.** (2025b) Restoration of native saltmarshes enhances carbon sequestration and mitigates warming effects following *Spartina alterniflora* removal. *J. Appl. Ecol.*, **62**, 2005–2017.

Wei, W., **Dai, Z.J.**, **Mei, X.F.**, **Gao, S.** and **Liu, J.P.** (2019) Multi-decadal morpho-sedimentary dynamics of the largest Changjiang estuarine marginal shoal: Causes and implications. *Land Degrad. Dev.*, **30**, 2048–2063.

Wei, W., **Dai, Z.J.**, **Pang, W.H.**, **Wang, J.** and **Gao, S.** (2020) Sedimentary zonation shift of tidal flats in a meso-tidal estuary. *Sed. Geol.*, **407**, 105749.

Wei, W., **Dai, Z.**, **Pang, W.**, **Wang, J.**, **Chen, Y.** and **Gao, S.** (2022) Frequency-dependent wave damping by tidal wetlands under storm conditions. *J. Hydrol.*, **613**, 128415.

Wei, Y., **van Maanen, B.**, **Xie, D.**, **Jiang, Q.**, **Zhou, Z.** and **Schwarz, C.** (2024) Mangrove-Saltmarsh ecotones: are species shifts determining eco-morphodynamic landform configurations? *Earth's Future*, **12**, e2024EF004990.

Wiberg, P.L., **Fagherazzi, S.** and **Kirwan, M.L.** (2020) Improving predictions of salt marsh evolution through better integration of data and models. *Ann. Rev. Mar. Sci.*, **12**, 389–413.

Willemsen, P.W.J.M., **Smits, B.P.**, **Borsje, B.W.**, **Herman, P.M.J.**, **Dijkstra, J.T.**, **Bouma, T.J.** and **Hulscher, S.J.M.H.** (2022) Modeling decadal salt marsh development: variability of the salt marsh edge under influence of waves and sediment availability. *Water Resour. Res.*, **58**, e2020WR028962.

Wu, W., **Lin, Z.**, **Chen, C.**, **Chen, Z.**, **Zhao, Z.** and **Su, H.** (2024) Tracking the dynamics of tidal wetlands with time-series satellite images in the Yangtze River Estuary, China. *Int. J. Digit. Earth*, **17**, 2330684.

Wu, Y., **Zhou, Z.**, **Dong, C.**, **Zheng, H.**, **Lin, W.**, **Gao, J.**, **Guo, P.**, **Gu, Y.**, **Le, T.** and **Bryan, K.R.** (2025) Impacts of exotic saltmarsh vegetation removal and native saltmarsh vegetation restoration on bed level change and surficial sediment distribution in an estuary wetland. *Case Rep. Med.*, **130**, e2024JF008119.

Xie, W., **He, Q.**, **Zhang, K.**, **Guo, L.**, **Wang, X.**, **Shen, J.** and **Cui, Z.** (2017) Application of terrestrial laser scanner on tidal flat morphology at a typhoon event timescale. *Geomorphology*, **292**, 47–58.

Xue, L., **Li, X.**, **Zhang, Q.**, **Yan, Z.**, **Ding, W.**, **Huang, X.**, **Ge, Z.M.** and **Yin, Q.** (2018) Elevated salinity and inundation will facilitate the spread of invasive *Spartina alterniflora* in the Yangtze River Estuary, China. *J. Exp. Mar. Biol. Ecol.*, **506**, 144–154.

Yang, S.L., **Friedrichs, C.T.**, **Shi, Z.**, **Ding, P.X.**, **Zhu, J.** and **Zhao, Q.Y.** (2003) Morphological response of tidal marshes, flats and channels of the outer Yangtze River mouth to a major storm. *Estuaries*, **26**, 1416–1425.

Yang, S.L., **Milliman, J.D.**, **Li, P.** and **Xu, K.** (2011) 50 000 dams later: erosion of the Yangtze River and its delta. *Global Planet. Change*, **75**, 14–20.

Yang, L., **Chi, Y.**, **Lu, H.**, **Sun, G.**, **Lu, Y.**, **Li, H.** and **Luo, Y.** (2024) Effects of the comprehensive elimination of *Spartina alterniflora* along China's coast on blue carbon and scenario prediction after ecological restoration. *J. Environ. Manage.*, **369**, 122283.

Yun, C.X. (2004) *Basic Law of the Recent Evolution of the Changjiang Estuary*. China Ocean Press, Beijing. (in Chinese with English abstract).

Zhang, Y., **Chen, R.** and **Wang, Y.** (2020) Tendency of land reclamation in coastal areas of Shanghai from 1998 to 2015. *Land Use Policy*, **91**, 104370.

Zhang, H., **Sun, T.**, **Zhou, Z.**, **Cao, H.**, **Qiu, J.** and **Huang, X.** (2022) Increased river flow enhances the resilience of spatially patterned mudflats to erosion. *Water Res.*, **220**, 118660.

Zhang, G., **Gu, J.**, **Hu, H.**, **Sun, M.**, **Shao, J.**, **Dong, W.**, **Liang, L.** and **Zeng, J.** (2024) Impact of coastal squeeze induced by erosion and land reclamation on salt marsh wetlands. *J. Mar. Sci. Eng.*, **13**, 17.

Zhou, Z., **Liu, Q.**, **Fan, D.**, **Coco, G.**, **Gong, Z.**, **Möller, I.**, **Xu, F.**, **Townend, I.** and **Zhang, C.** (2021) Simulating the role of tides and sediment characteristics on tidal flat sorting and bedding dynamics. *Earth Surf. Proc. Land.*, **46**, 2163–2176.

Zhou, X., **Zuo, Y.**, **Zheng, K.**, **Shao, C.**, **Shao, S.**, **Sun, W.**, **Yang, S.**, **Ge, W.**, **Wang, Y.** and **Yang, G.** (2024) Monitoring the invasion of *S. alterniflora* on the Yangtze River Delta, China, using time series Landsat images during 1990–2022. *Remote Sens.*, **16**, 1377.

Zhu, Z., **Zhang, L.**, **Wang, N.**, **Schwarz, C.** and **Ysebaert, T.** (2012) Interactions between the range expansion of saltmarsh vegetation and hydrodynamic regimes in the Yangtze Estuary, China. *Estuar. Coast. Shelf Sci.*, **96**, 273–279.

Manuscript received 7 April 2025; revision accepted 19 December 2025

Supporting Information

Additional information may be found in the online version of this article:

Fig. S1. (A) Field observation using the terrestrial laser scanner (TLS, Riegl VZ-4000). (B) RTK-measured intertidal elevation sites in the South Nanhui wetland. (C) Comparison between RTK-measured and TLS-measured intertidal elevations.

Fig. S2. (A–G) Salt marsh distribution and expansion in the Nanhui wetlands between 2016 and 2022, with the entire area divided into eight sub-areas according to geographical conditions and artificial groins. (H–J) Annual changes in salt marsh areas.